Localization of I-BAR domain proteins in invasive cancer cells

Kirsi Sepponen

Pro Gradu

Jyväskylän yliopisto

Bio- ja ympäristötieteiden laitos

Solu- ja molekyylibiologia

24.5.2011

Preface

This study was conducted in the group of Pekka Lappalainen at the Institute of Biotechnology, University of Helsinki. I wish to express my gratitude to my supervisor professor Pekka Lappalainen for giving me the opportunity to do research in his group and for all the excellent advice and help during the writing process. I owe my warmest thanks to PhD. Juha Saarikangas for all the excellent technical and non-technical guidance and for all the patience during my project. Juha supported me at times of desperation and was always eager to find answers to my questions.

I am deeply grateful to the whole group of Pekka Lappalainen for all the valuable advice related to my project and life in general and for the helpful attitude during the project. I will miss the great atmosphere I had the chance to experience. I would also like to thank all the members of research groups at the 5th floor at the Institute of Biotechnology, with whom I had encouraging academic conversations.

I would like to thank the staff working in the department of Biology and Environmental Science for the excellent teaching and advice during my studies.

Finally, I am grateful to my family, who helped me to move to another city once again for this project and who has taken care of my wellness during my studies.

University of Jyväskylä **Abstract of Master's thesis**
Faculty of Mathematics and Science

Author:	Kirsi Sepponen
Title of thesis:	Localization of I-BAR domain proteins in invasive cancer cells
Finnish title:	I-BAR domeeni-proteiinien sijainti invasiivisissa syöpäsoluissa
Date:	24.5.2011 **Pages:** 67
Department:	Department of Biological and Environmental Science
Chair:	Cell and Molecular Biology
Supervisor(s):	Prof. Pekka Lappalainen and PhD Juha Saarikangas, Institute of Biotechnology, University of Helsinki
Place of performance:	Institute of Biotechnology, University of Helsinki

Abstract:

An important step in cancer metastasis is the ability of the cancer cells to degrade the surrounding extracellular matrix (ECM) and migrate through it. To accomplish this, invasive cancer cells generate protrusive structures called invadopodia, which are dynamic cell protrusions that secrete matrix metalloproteinases (MMPs) responsible for the degradation of the ECM.

Invadopodia formation employs the actin polymerization machinery and several cell adhesion, signal transduction and matrix degradation proteins. In addition, mechanisms involving membrane deformation may play a major role in their formation. Recently, an evolutionary conserved group of proteins involved in the formation of cell protrusions was characterized. These proteins were found to contain an inverse Bin-Amphiphysin-Rvs167 (I-BAR) domain. The I-BAR domain is capable of bending the plasma membrane outwards and via accessory domains, the I-BAR proteins link this membrane bending activity to actin cytoskeleton remodeling to generate cell protrusions.

In the present study, the aim was to examine the localization of I-BAR domain proteins in invasive cancer cell lines. First, I studied the expression of the members of the I-BAR gene family (ABBA, IRTKS, IRSp53) in MDA-MB-231 breast cancer cells and SNB-19 glioma cells by reverse transcription polymerase chain reaction **(**RT-PCR) and Western blotting. The results indicated that I-BAR domain proteins were expressed at the messenger RNA (mRNA) and protein level in both cell lines.

Then, to investigate the sub-cellular localization of these proteins to invasive sites, an ECM degradation assay was set up to distinguish invadopodias from other actin-rich sub-cellular structures. Using this assay, the localization of both endogenous and green fluorescent protein (GFP)-tagged I-BAR domain proteins to invadopodia was studied by light microscopy. Endogenous I-BAR domain proteins were examined both in two dimensional (2D) and three dimensional (3D) environments, but the antibodies used in this study appeared not to be suitable for their detection. However, the intensity profiles of invadopodia showed that in cells expressing I-BAR domain proteins fused to a GFP, these proteins accumulated either on the edge or at the centre of an invadopodium.

The results suggest that the I-BAR domain proteins are likely to be recruited to distinct sites of invadopodia where they can induce or stabilize plasma membrane curvature and link it to actin cytoskeleton remodeling during the formation of invasive cell protrusions.

Keywords: invadopodium, I-BAR domain, matrix degradation, MDA-MB-231

Jyväskylän yliopisto **Pro gradu - tutkielman tiivistelmä**
Matemaattis-luonnontieteellinen tiedekunta

Tekijä: Kirsi Sepponen
Tutkielman nimi: I-BAR domeeni-proteiinien sijainti invasiivisissa syöpäsoluissa
English title: Localization of I-BAR domain proteins in invasive cancer cells
Päivämäärä: 24.5.2011 **Sivumäärä:** 67
Laitos: Bio- ja ympäristötieteiden laitos
Oppiaine: Solu- ja molekyylibiologia
Tutkielman ohjaaja(t): Prof. Pekka Lappalainen ja FT Juha Saarikangas, Biotekniikan instituutti, Helsingin yliopisto
Tutkielman suorituspaikka: Biotekniikan instituutti, Helsingin yliopisto

---

Tiivistelmä:

Syövän etäpesäkkeiden muodostumisen kannalta on oleellista syöpäsolujen kyky hajottaa ympäröivää soluväliainetta (ECM) ja vaeltaa sen läpi. Invasiiviset syöpäsolut muodostavat ulokkeita, joita nimitetään invadopodioiksi. Ne ovat dynaamisia rakenteita, jotka erittävät soluväliainetta hajottavia metalloproteaasi-entsyymejä (MMPs).

Invadopodioiden muodostumiseen tarvitaan lisäksi aktiinin polymerisaatioon, soluadheesioiden kehittymiseen ja signaalivälitykseen liittyviä molekyylejä. Myös solukalvon muokkaamiseen liittyvillä mekanismeilla saattaa olla osuutta invadopodioiden syntymiseen. Hiljattain on löydetty evolutiivisesti konservoitunut proteiiniperhe, joka osallistuu solun ulokkeiden kehittymiseen. Kyseiseen proteiiniperheeseen kuuluvien proteiinien rakenne sisältää käänteisen Bin-Amphiphysin-Rvs167 (I-BAR) -domeenin, jonka avulla solukalvo taipuu ulospäin. Avustavien proteiinien välityksellä I-BAR domeeni on yhteydessä aktiinitukirankaan, jota tarvitaan solun ulokkeiden syntymiseen.

Tämän tutkimuksen tavoitteena oli selvittää I-BAR domeeni-proteiinien sijaintia invasiivisissa syöpäsoluissa. Aluksi selvitin eräiden I-BAR geeniperheen jäsenten (ABBA, IRTKS, IRSp53) ilmentymistä käänteiskopioijaentsyymiin perustuvalla polymeraasiketjureaktiolla (RT-PCR) ja Western-blottauksella MDA-MB-231 rintasyöpäsolulinjassa ja SNB-19 glioomasolulinjassa. Tulosten perusteella I-BAR domeeniproteiineja ilmentyy lähetti- RNA (mRNA) ja proteiinitasolla kummassakin solulinjassa.

Soluväliaineen hajoamiseen perustuvalla menetelmällä tutkin I-BAR domeeni-proteiinien sijaintia soluissa. Menetelmä oli käyttökelpoinen invadopodiarakenteiden erottamiseen muista aktiinia sisältävistä solun rakenteista. Kyseisen menetelmän avulla selvitettiin endogeenisten ja vihreään fluoresoivaan proteiiniin (GFP) liitettyjen I-BAR domeeni-proteiinien sijaintia soluissa valomikroskopiaa hyödyntäen. Endogeenisten proteiinien sijaintia selvitettiin kaksiulotteisessa (2D) ja kolmiulotteisessa (3D) ympäristössä, mutta proteiinien leimaamisessa käytetyt vasta-aineet eivät kokeitteni perusteella soveltuneet tähän tutkimukseen. Kuitenkin soluissa, joissa ilmentyi I-BAR domeeni-proteiini GFP:hen liittyneenä, nämä proteiinit sijoittuivat joko invadopodian keskelle tai reunoille.

Näiden tulosten perusteella I-BAR domeeni-proteiinit saattavat aktivoida tai tasapainottaa solukalvon rakennetta invadopodioissa ja mahdollisesti liittävät solukalvon aktiinitukirankaan, jolloin solun ulokkeiden muodostumisen on mahdollista.

Avainsanat: invadopodia, I-BAR-domeeniproteiini, soluväliaineen hajoaminen, MDA-MB-231

Table of contents

Abbreviations

aa.	amino acid
ABBA	F-actin bundling protein with BAIAP2 homology
ADP	adenosine 5'-diphosphate
Arp2/3	actin-related protein 2/3
ASAP	Arf guanine triphosphatase-activating protein
ATP	adenosine 5'-triphosphate
BAR	Bin-Amphiphysin-Rvs167
BSA	bovine serum albumin
Cdc42	Cell division control protein 42 homolog
cDNA	complementary DNA
CRIB	partial-Cdc42/Rac interactive binding motif
C-terminus	carboxy-terminus of a protein
3D	three dimensional
2D	two dimensional
DNA	deoxyribonucleic acid
E. coli	*Escherichia coli*
ECM	extracellular matrix
EGF	epidermal growth factor
EMT	epithelial-mesenchymal transition
EspFU	enterohemorrhagic *E. coli* secreted protein FU
F-actin	filamentous actin
F-BAR	FER-CIP4 homology-BAR
g	gravitational force
G-actin	globular actin, actin monomer
GFP	green fluorescent protein
GST	glutathione S-transferase
I-BAR	inverse BAR
IRSp53	insulin receptor tyrosine kinase substrate of 53 kilodalton

IRTKS	insulin receptor tyrosine kinase substrate
kb	kilo base
kDa	kilodalton
LB	Luria-Bertani
MIM	missing-in-metastasis
MMP	matrix metalloproteinase
mRNA	messenger RNA
MT1-MMP	membrane type 1 matrix metalloproteinase
Nck1	non-catalytic region of tyrosine kinase adaptor protein 1
N-terminus	amino-terminus of a protein
N-WASP	neural Wiskott-Aldrich Syndrome protein
PBS	phosphate-buffered saline
PCR	polymerase chain reaction
$PI(4,5)P_2$	phosphatidylinositol-4,5-bisphosphate
RNA	ribonucleic acid
RT	room temperature
RT-PCR	reverse transcription polymerase chain reaction
SH3	Src homology 3
Tir	translocated intimin receptor
Toca-1	transducer of Cdc42-dependent actin assembly
TBS	Tris-buffered saline
U	unit
WH2	Wiscott-Aldrich syndrome protein homology 2
WIP	WASP-interacting protein
WWB	tryptophan, tryptophan -domain binding motif

Introduction

1.1 Cancer

Malignant cancer is defined by uncontrolled growth of abnormal cells, which are able to invade to the surrounding tissue (Alberts et al., 2008). Cancer is one of the most devastating diseases in the human population. In 2008, it was estimated to be the cause of death for over 7 million people, and approximately 13 million new cases appeared in a year worldwide. The most diagnosed cancers were breast cancer in females and lung cancer in males, while both of them resulted in most of the cancer deaths per each sex (Jemal et al., 2011).

Cancer is caused by both environmental/acquired and internal factors, where the former group results in the majority of cancer cases. Environmental/acquired sources include for example various chemicals, radiation, infectious agents and diet, while the internal sources comprise inherited mutations, hormones and immune system malfunctions. Only 5-10 % of cancers have been estimated to be inherited and various cancers are associated with genetic defects, which originally derive from the environment (for review see Anand et al., 2008).

Six core capabilities of cancer are acquired during cancer formation. One of these is the ability of malignant cells to sustain proliferative signaling, which can be achieved by several ways. Currently known mechanisms include stimulation of normal cells to produce growth factors for the benefit of cancer cells, induction of autocrine signaling pathways, deregulation of receptor signaling by sensitizing the cell to growth factors, somatic mutations that activate downstream pathways and disruption of negative-feedback circuits. The other core capabilities involve evading growth suppressors, activating invasion and metastasis, enabling replicative immortality, resisting cell death and inducing angiogenesis, which is referred to formation of novel blood vessels. The acquisition of these capabilities is facilitated by both genome instability and tumour-promoting inflammation (for review see Hanahan and Weinberg, 2011).

Most cancers are genetically unstable, which means that cancer cells accumulate genetic alterations more rapidly than normal cells. These alterations include single point mutations in the deoxyribonucleic acid (DNA) sequence or changes at the chromosomal level causing translocations, amplifications or deletions of the genetic material. Multiple mutations are required for malignant transformation, where normal cells acquire properties of cancer cells. These mutations originate from mistakes in DNA synthesis or from copying DNA sequence, which has not been corrected by the cellular DNA repair system (for reviews see Lengauer et al., 1998; Loeb and Loeb, 2000).

In addition, inflammation fosters many capabilities of cancer cells by supplying molecules to the tumour microenvironment, which consists of tumour cells, tumour stem cells, progenitor cells, tumour-antagonizing and tumour-promoting inflammatory cells, cancer-associated fibroblasts, pericytes and endothelial cells. The molecules delivered by inflammatory cells comprise of growth factors sustaining proliferative signaling, survival factors that limit cell death and molecules contributing to angiogenesis, metastasis and invasion. In addition, inflammatory cells release mutagens, which speed up the mutation rate of nearby cancer cells (for review see Hanahan and Weinberg, 2011).

1.2 Cancer metastasis and epithelial-mesenchymal transition (EMT)

Metastasis describes a process where the cancer spreads from the site of the primary tumor to distant locations in the body. It requires somatic evolution of genetically heterogeneous lineages of cancer cells under selective pressures. These selective pressures include both intrinsic factors such as the expression of apoptotic, growth inhibitory and senescence pathways and extrinsic factors comprising of extracellular matrix (ECM) components, basement membranes, the immunological defence, reactive oxygen species, the limited availability of nutrients and oxygen. The cancerous cells which have evolved traits that enable them to overcome those barriers dominate the cancer making it susceptible for metastatic progression (for review see Gupta and Massague., 2006).

In most cases, the appearance of metastases implies poor prognosis among cancer patients. As the molecular mechanisms underlying the steps of metastasis are still incompletely characterized, they have gained a wide interest among the cancer research community in the past few years (for review see Gupta and Massague., 2006).

The distinct stages of metastasis include detachment of tumor cells from the primary tumor site and the invasion of these cells into the surrounding tissue, intravasation through endothelial barriers into blood or lymphatic vessels, dissemination and survival in the blood circulation without destruction by mechanical forces or immune system cells, attachment to a target organ, extravasation into the surrounding tissue and growth of the secondary tumor. Each of these steps involves partially distinct sets of molecules and also the properties of the metastasising tumor cell itself change on its way from the primary tumor site to the new localization (for reviews see Gupta and Massague, 2006; Yilmaz and Christofori, 2009).

1.2.1 EMT

Initiation of metastasis involves detachment of the tumor cells from the primary tumor site, which requires disruption of cell-cell contacts, remodeling cell-cell and cell-matrix adhesion sites and migration of the cells in ECM. During these steps the cell undergoes a reversible process called EMT, where the cell loses its epithelial phenotype and acquires mesenchymal characteristics. During EMT, the cell converts from a non-motile and polarized epithelial morphology into a motile, highly invasive mesenchymal cell type. Upon transition the molecular composition of the cell experiences drastic changes. One of the significant changes includes the silencing of E-cadherin expression and loss of function to be replaced by the induction of N-cadherin expression. As a result, the adhesive properties of the cell change and it acquires affinity for mesenchymal cells, such as vascular endothelial cells and fibroblasts (for review see Yilmaz and Christofori, 2009). This process is called cadherin switch, and it takes place also in non-pathological conditions such as during development of certain tissues (Nakagawa and Takeichi, 1995).

1.3 Actin in cancer cells

Actin is an abundant and essential protein in all eukaryotic cells. Actin plays a role in cellular movements, providing tracks for intracellular trafficking and force to drive cellular motility. In addition to these functions, actin also provides the cells internal mechanical support and defines the shape of the cell together with intermediate filaments and microtubules. Actin polymer referred to as filamentous actin (F-actin) is a polar structure that consists of helically arranged actin monomer (G-actin) subunits. G-actin binds either adenosine 5'-triphosphate (ATP) or adenosine 5'-diphosphate (ADP) (for review see Pollard and Cooper, 2009).

Upon polymerization ATP-bound actin is favoured (Bray, 2001). Almost immediately after the subunits have been incorporated into the growing filament, one of the phosphate groups on actin bound ATP is dissociated and the remaining ADP stays at the subunit, which leads to a conformational change. This results in a less stable actin filament structure, which subsequently induces depolymerisation (Alberts et al. 2008). The disassembly of ADP-actin filaments is enhanced in cells by several regulatory proteins (for review see Pollard and Cooper, 2009).

The polarity of the actin molecule is a consequence of the same orientation of the subunits in the filament and results in two distinct ends of the molecule termed barbed (+) end and pointed (-) end. The barbed end grows 5-10 times faster than the pointed end due to the preference of ATP-bound G-actin to incorporate to it. On the contrary, at the pointed end the subunit addition is slower than hydrolysis. At steady-state G-actin concentration the incorporation of G-actin at the barbed end and their dissociation at the pointed end is termed treadmilling (Bray, 2001).

The formation of new actin filaments requires branching of the existing filaments, severing of a filament to create two ends or nucleation of a completely new filament from G-actin (for review see Pollard and Cooper, 2009). Actin-related protein 2/3 (Arp2/3) complex consists of seven subunits including actin-related proteins 2 and 3 and it has a role in nucleating new

filaments at ~70 degree angles from the side of a pre-existing filament (Mullins et al., 1998; Amann and Pollard, 2001). In addition to Arp2/3-complex, there are many other proteins that can nucleate the assembly of new actin filaments, including formins and proteins containing multiple Wiskott-Aldrich syndrome protein homology 2 (WH2)-domains (for review see Qualmann and Kessels, 2009). In cells, the assembly and disassembly of actin is regulated by a vast number of actin-binding proteins. One of the most central regulator of actin dynamics is cofilin, which promotes treadmilling by severing actin filaments to create free barbed ends and by promoting actin depolymerisation. As a result, the number of short filaments and G-actin increases, which subsequently stimulates actin polymerization (Lappalainen and Drubin, 1997; Ghosh et al., 2004; Kiuchi et al., 2007; Pavlov et al., 2007).

Actin polymerization plays a major role in the formation of cell protrusions at the leading edge of the cell. Such protrusions are required in cell locomotion, and they include sheet-like lamellipodia consisting of branched actin filaments (Svitkina and Borisy, 1999) and filopodia, where filaments have arranged into parallel bundles (Lewis and Bridgman, 1992). Quite recently a unique form of membrane protrusions referred to as an invadopodium was identified in various tumor cells (Chen, 1989; Coopman et al., 1996; Clark et al., 2007), which requires actin cytoskeleton for its formation and function (Yamaguchi et al., 2005; Artym et al., 2006; Baldassarre et al., 2006).

1.4 Invadopodia in invasive cancer cells

Malignant cancer cells are well-known for their invasiveness, which requires matrix degradation and cellular motility through the tissue (Kikuchi and Takahashi, 2008). The invasion and migration of tumour are driven by cellular protrusions in the direction of cancer cell movement (Yamaguchi et al., 2005). Invadopodia are actin-based structures of transformed cells and tumour cells that extend from the ventral surface of the cell into the ECM mediating proteolysis of ECM components (Chen, 1989; Mueller and Chen, 1991; Kelly et al., 1998; Yamaguchi et al., 2005). Invadopodia are capable of degrading several constituents of ECM such as fibronectin, laminin, type IV and type I collagens (Chen, 1989;

Mueller et al., 1992; Kelly et al., 1994) and hence, invadopodia-mediated proteolysis of ECM has been suggested to help cancer cells to invade into the surrounding ECM (Chen, 1996; Kelly et al., 1998). Invadopodial structures have been found from a variety of cell types including human melanoma cells (Tague et al., 2004), human breast cancer cells (Coopman et al., 1996; Artym et al., 2006), glioma (Angers-Loustau et al., 2004; Chuang et al., 2004), head and neck squamous cell carcinoma (Clark et al., 2007) and transformed chicken fibroblasts (Chen, 1989).

Invadopodia were originally found in embryonic chick fibroblasts transformed by the viral sarcoma oncogene (Chen, 1989). This gene encodes a constitutively active non-receptor tyrosine kinase, which was able to stimulate invadopodia formation in fibroblasts where invadopodia are naturally absent (Chen et al., 1984). Later, it has been observed that massive tyrosine phophorylation of membrane bound proteins takes place in invadopodia possibly contributing to the formation of invadopodia (Mueller et al., 1992). Invadopodia are 0.5 µm to 2 µm in diameter, while their length is 1-7 µm, depending on the stage of maturation (Schoumacher et al., 2010). They are capable of self-organizing into ring-like rosettes, which are essential for efficient matrix degradation, possibly due to the increased local concentration of matrix proteases (Badowski et al. 2008). Similar structures are found from podosomes, which are closely related to invadopodia (for review see Linder, 2007).

Podosomes are tubular invaginations, which form at the ventral plasma membrane (Ochoa et al., 2000). They are found from monocytic (Linder et al., 1999; Burns et al., 2001; Destaing et al., 2003), endothelial (Osiak et al., 2005; Tatin et al., 2006) and smooth muscle cells (Hai et al. 2002; Burgstaller and Gimona, 2005). Podosomes are smaller in size and more numerous per cell than invadopodia (for review see Linder, 2007). In addition, podosomes have a half-life of several minutes (Destaing et al., 2003; Evans et al., 2003), while invadopodia have been observed to persist longer, up to several hours (Yamaguchi et al., 2005). Podosomes have shown degradation of ECM components in various cell types (Mizutani et al., 2002; Burgstaller and Gimona, 2005; Tatin et al., 2006) but the efficiency of degradation is generally weaker than in invadopodia. Due to the quicker turnover rate and higher number of

podosomes the degradation of the substratum is broader and more shallow in comparison to invadopodia, which penetrate deeply into the ECM and focus their degradation activity at specific sites. Although invadopodia and podosomes share several similarities and podosomes have been suggested to develop into invadopodia, the transition process has not been experimentally shown (for review see Linder, 2007).

1.4.1 Invadopodia formation

In the past few years, the different stages in invadopodia formation have been determined at the molecular level. There are several proteins associated with invadopodia, which can be divided into four functional groups (for review see Buccione et al., 2004). The first group consists of structural proteins including actin and components interacting with actin, such as Arp2/3, neural Wiskott-Aldrich Syndrome protein (N-WASP), Cell division control protein 42 homolog (Cdc42), Rac, a non-catalytic region of tyrosine kinase adaptor protein 1 (Nck1), WASP-interacting protein (WIP), cofilin and a cortical actin binding protein referred to as cortactin (Nakahara et al., 2003; Lorenz et al., 2004; Yamaguchi et al., 2005; Artym et al., 2006). The second group comprises several integrins, which mediate invadopodia-ECM interaction. As an example, β1 integrin localizes in invadopodia of transformed fibroblasts (Mueller and Chen, 1991), melanoma cells (Nakahara et al., 2003) and invasive breast cancer cells (Bowden et al., 1999) and has been suggested to participate in matrix degradation, stabilization of invadopodia and invasiveness of cancer cells (Nakahara et al., 1996; Mueller et al., 1999). Integrins and the proteins associated with them are surrounding the actin-rich core of an invadopodium forming a structure called an adhesive ring (Fig. 1) (for review see Yilmaz and Christofori., 2009). The third group includes signaling proteins such as Ras – related guanosine triphosphatases, which have a role in regulating the actin cytoskeleton, while the fourth group consists of matrix metalloproteinases (MMPs), which are zinc-derived endopeptidases that degrade ECM components and activate each other. They are divided into soluble MMPs, which become activated once they exit the cell and membrane-type MMPs, which are transmembrane proteins (Artym et al., 2006; for review see van Hinsbergh et al., 2006). Membrane type 1 matrix metalloproteinase (MT1-MMP) was found from invadopodia of melanoma cells, where it stimulated degradation of ECM components and invasion of

cancer cells. As a transmembrane protease MT1-MMP is probably required to induce focused activation of MMPs (Nakahara et al., 1997). MT1-MMP degrades ECM components directly or proteolytically activates soluble or ECM bound MMP2 at the sites of invadopodia (Imai et al., 1996; Pei and Weiss., 1996; Deryugina et al., 2001). Also MMP9 localizes to invadopodia (Bourguignon et al., 1998) and these three proteases have been suggested to belong to the standard set of proteases required for ECM degradation (for review see Linder, 2007).

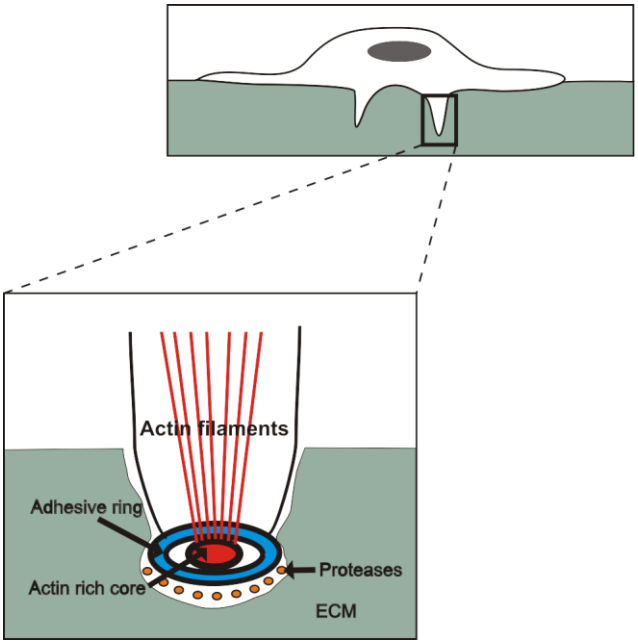

Figure 1. Structure of an invadopodium. Invadopodia include an actin- rich central core and an outer adhesive ring, where integrins are located. In the core region, actin, cortactin and MT1-MMP participate in invadopodia maturation (for review see Yilmaz and Christofori, 2009). MT1-MMP degrades ECM directly or alternatively interacts with αvβ3-integrin located at the adhesive ring. This event results in proteolytic activation of immature MMP2 and subsequent collagen degradation (Imai et al., 1996; Pei and Weiss., 1996; Deryugina et al., 2001). The proteolytic activity is most efficient at the tips of invadopodia, where it assists invasion by weakening ECM resistance (Artym et al., 2006). The figure is modified from the review by Yilmaz and Christofori (2009).

Yamaguchi et al. (2005) have shown that invadopodia are dynamic structures which have a lifetime from a few minutes to several hours. Several signaling molecules can initiate the formation of invadopodia (for review see Yilmaz and Christofori., 2009). These are for example epidermal growth factors (EGFs) activating an EGF receptor (Yamaguchi et al., 2005) (Fig. 1) and laminin G peptides interacting with α6β1-integrins on the cell membrane (Nakahara et al., 1996). Much is still not known about the signaling cascades required for the invadopodia formation. However, studies have shown the importance of certain actin-associated molecules in the initiation of invadopodia formation. Such molecules are Nck1 and Cdc42, that are recruited and activated by a currently unknown mechanism, which possibly involves accessory molecules downstream from the EGF receptor. First, Nck1 delivers N-

WASP-WIP complex to the sites of invadopodia formation, while Cdc42 activates N-WASP probably via Toca-1 (transducer of Cdc42-dependent actin assembly), which directly binds to both molecules (Yamaguchi et al., 2005). In support to this hypothesis, Toca-1 was recently found to have a regulatory role in Cdc42-dependent actin polymerization (Ho et al., 2004). Next, N-WASP is activated by releasing the autoinhibitory conformation of the molecule (Yamaguchi et al., 2005). Finally, activated N-WASP promotes actin polymerization by directly binding to Arp2/3 complex via its C-terminal end (Rohatgi et al., 1999).

Actin polymerization has been proposed to anchor the dynamic invadopodia at the sites of maturation (Yamaguchi et al., 2005) and together with cortactin actin localizes to ventral puncta where they recruit MT1-MMP to form pre-invadopodia. Pre-invadopodia stage is followed by additional recruitment of cortactin, actin and MT1-MMP, which together lead to the formation of mature invadopodia as indicated by the degradation of an underlying matrix (Artym et al., 2006). During the formation of an actin-rich core and the subsequent elongation process of an invadopodium, the same coreset of actin binding proteins are used as in lamellipodia and filopodia regulation (Schoumacher et al., 2010). Cofilin possibly has a role in invadopodia maturation as it participates in the formation of new actin filaments promoting actin assembly and elongation of invadopodia (Yamaguchi et al., 2005).

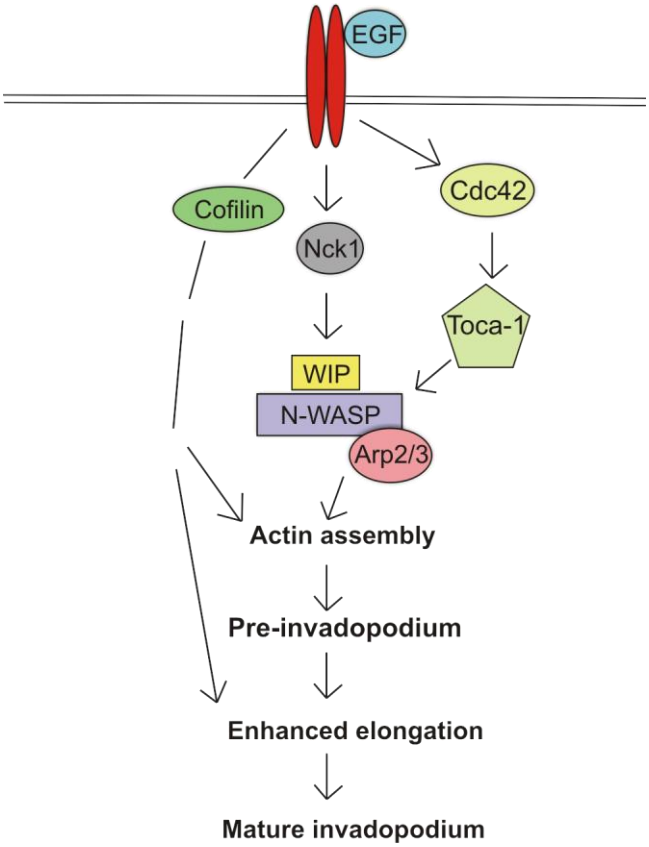

Figure 2. Schematic model for signaling events underlying invadopodia formation. Binding of extracellular EGF molecule to its transmembrane receptor leads to activation of Nck1, Cdc42 and cofilin. A complex consisting of WIP, N-WASP and Arp2/3 is recruited by Nck1. Cdc42 activates N-WASP via Toca-1, which stimulates Arp2/3 mediated actin filament assembly and initiates the formation of invadopodia. Matrix metalloproteases are required for ECM degradation and the subsequent formation of mature invadopodia, while cofilin promotes actin depolymerization during maturation of invadopodia. The figure is modified from Yamaguchi et al. (2005).

Microtubules and intermediate filaments enter the mature invadopodia. Microtubules are required for the elongation of an invadopodium after it has reached the length of 5 µm (Kikuchi and Takahashi, 2008; Schoumacher et al., 2010). It has been suggested that microtubules function in MMP trafficking and this hypothesis has been supported by their presence in mature invadopodia (Schoumacher et al., 2010).

Interestingly, intermediate filaments vimentin and keratin were found only from mature invadopodia (Schoumacher et al., 2010). It has been shown that during EMT and loss of cell-cell contacts the expression of vimentin is initiated, while there is a switch in keratin expression (Mendez et al., 2010). Moreover, vimentin is an essential component for the motility and invasion of prostate cancer cells proposing that intermediate filaments stabilize mature invadopodia during invasion of ECM (Zhao et al., 2008; Schoumacher et al., 2010).

In addition to actin polymerization, invadopodia may involve concomitant membrane deformation (Albiges-Rizo et al., 2009). Several membrane deforming proteins exist in nature and these are discussed in detail in the following chapter.

1.5 Bin-Amphiphysin-Rvs167 (BAR) domain superfamily

The BAR domain superfamily consists of proteins that regulate membrane remodeling in eukaryotes. These proteins can be divided into three subfamilies based on their distinct structural features and phylogeny. These subfamilies contain either a BAR/N-BAR, FER-CIP4 homology (F-BAR) or inverse BAR (I-BAR) domains that bind the target membrane by electrostatic interactions and in some cases also insert a helix into the membranes (for review see Frost et al., 2009 and Suetsugu et al., 2010)

Most BAR domain superfamily members are multidomain proteins including an actin-binding WH2 domain, a Src homology 3 (SH3) domain and Rho guanosine nucleotide exchange factor/ guanosine triphosphatase-activating protein domains, which are all essential for linking BAR domain proteins to the cytoskeletal actin dynamics (for review see Saarikangas et al., 2010). WH2 domain is generally known as an ATP-G-actin binding domain, which is found from several regulators of actin cytoskeleton (for review see Paavilainen et al., 2004), while SH3 domains bind to proline-rich sequences present in various proteins (for review see Macias et al., 2002).

1.6 BAR domain protein family

The BAR domain is a homodimeric structure, where each monomer contains three antiparallel α-helices that form a banana-shaped six-helix bundle (Peter et al., 2004). Arfaptin BAR was the first BAR domain that was structurally determined (Tarricone et al., 2001), although at that time it was not known to have membrane-binding activity. Since, several proteins with BAR domain have been identified. BAR domain has a positively charged concave surface that binds

to the negatively charged lipid groups on the plasma membrane inducing membrane bending and subsequent tubulation (Peter et al., 2004).

The N-BAR domain proteins are a subset of BAR domain proteins that additionally insert an amino-terminal (N-terminal) amphipathic helix containing hydrophobic amino acids (aa.) into the membrane to aid the membrane deformation activity and to strengthen the BAR domain-membrane interaction (Gallop et al., 2006; Masuda et al., 2006).

The BAR domain protein, an Arf guanine triphophatase-activating protein (ASAP) has been linked to the formation of invadopodia and podosomes. This was observed by reduction of ASAP expression levels and by mutational studies, which inhibited formation of protrusions (Bharti et al., 2007).

1.7 F-BAR domain protein family

The F-BAR domain contains five α-helices per monomer and shares weak sequence homology with BAR domains. In addition, both protein domains share powerful membrane –deforming activity *in vivo* and *in vitro*. F-BAR domain can be found from many actin binding proteins as an evolutionarily conserved FCH domain and as an adjacent coiled-coil region, hence the name extended FCH. (Itoh et al., 2005; Tsujita et al., 2006)

In comparison to the BAR domain, F-BAR domains induce membrane tubules with larger diameter than proteins containing BAR domains. This is due to the more gently curved and more elongated structure of the F-BAR domain (Shimada et al., 2007). Tsujita et al. (2006) confirmed the role of F-BAR domain in the formation of endocytic vesicles by knockdown of F-BAR domain and by localization studies. Moreover, recent findings suggest that a subgroup of F-BAR domain proteins induces negative membrane curvature. Two F-BAR domain containing proteins Fes and Fer have been shown to participate in cell protrusions and cell migration (Itoh et al., 2009). Guerrier et al. (2009) observed that the F-BAR domain of SLIT-ROBO Rho guanine triphophatase activating protein 2 induces negative membrane curvature

in vitro and stimulates filopodia-like protrusions *in vivo*. In addition, the WASP-family verprolin-homologous protein (WAVE)-associated Rac guanosine triphosphatase activating protein contains an inverse F-BAR, which mediates the formation of protrusions analogous to filopodia during spine development and which is associated with long-term memory in mice (Carlson et al., 2011).

1.8 I-BAR domain protein family

The I-BAR domain was originally found from five proteins including mammalian missing-in-metastasis (MIM) and insulin receptor tyrosine kinase substrate of 53 kilodalton (kDa) (IRSp53) (Yamagishi et al., 2004; for review see Scita et al., 2008). The sequence analyses and predicted secondary structures confirmed that I-BAR domain is highly conserved in all vertebrates and has ancestral homologs in invertebrates *Caenorhabditis elegans* and *Drosophila melanogaster* (Yamagishi et al., 2004; for review see Scita et al., 2008 and Zhao et al., 2011).

The I-BAR domain family is a member of BAR superfamily domain and it consists of IRSp53-like and MIM-like domains. Despite that I-BAR domains of IRSp53 and MIM have only ~19 % identical sequences, these domains are structurally very similar showing variation mainly toward the N- and C-terminal ends and in the loop region between helices 2 and 3 (Millard et al. 2005, Lee et al., 2007). The I-BAR domain is a dimer consisting of three alfa helices that form an antiparallel inverse BAR domain shaped structure (Lee et al., 2007), which affects its functional properties in comparison to BAR and F-BAR domain proteins (Mattila et al., 2007).

The I-BAR domain binds to phopholipids, especially phosphatidylinositol-4,5-bisphosphate ($PI(4,5)P_2$) (Suetsugu et al., 2006, Mattila et al., 2007). The domain has been shown to tubulate membranes *in vitro* and to induce filopodia in cultured cells (Yamagishi et al., 2004; Suetsugu et al., 2006; Mattila et al., 2007). The major functional difference between BAR and I-BAR domains is the direction of the membrane deformation, which can be explained by

different topology of the membrane binding surfaces between the BAR and I-BAR domains (Mattila et al., 2007). BAR domain proteins bind the plasma membrane by their concave surface while I-BAR domain proteins use their convex surface to deform the membrane. Both types of domains are also capable of inducing PI(4,5)P_2-clustering upon binding, but the biological function of this activity is not known (Saarikangas et al., 2009).

The distinct I-BAR domains have been shown to deform cellular membranes either mainly through electrostatic interactions or inserting an amphipathic α-helix into the lipid bilayer. In the previous studies by Saarikangas et al. (2009) insulin receptor tyrosine kinase substrate (IRTKS) and IRSp53 proteins have been observed to use electrostatic interactions for membrane binding and subsequent bending, while two other domains, F-actin bundling protein with BAIAP2 homology (ABBA) domain and MIM I-BAR domain, additionally insert an amphipathic α -helix into the membrane. Moreover, there are differences in the tubule diameters induced by different I-BAR domains. The tubules induced by IRSp53 and IRTKS were narrower than the ones induced by MIM and ABBA. This is due to the membrane insertion, which significantly increases the diameter of the tubule. In addition, the I-BAR domains inserting the helix into the membrane induced filopodia more efficiently than the I-BAR domains functioning only via electrostatic interactions.

The results from studies determining actin bundling activity of I-BAR domain have been controversial. Several studies suggested that I-BAR domain binds to F-actin and bundles it to form cellular protrusions (Yamagishi et al., 2004; Gonzalez-Quevedo et al., 2005; Millard et al., 2005), while other studies have contrasted these results by showing that the domain has no F-actin bundling activity in physiological ionic conditions (Lee et al., 2007; Mattila et al., 2007; Saarikangas et al., 2009).

1.8.1 The IRSp53 subfamily

IRSp53 subfamily consists of three members: IRSp53, IRTKS and FLJ22582 (for review see Zhao et al., 2011). Figure 3. illustrates the domain structures of the I-BAR domain proteins. All IRSp53 subfamily proteins contain an I-BAR domain in their N-terminal end and a SH3

domain in their C-terminal end. SH3 domain binds to several signalling proteins such as WAVE2, which mediates in lamellipodia formation (Miki et al., 2000) and an Ena/VASP family member mammalian enabled protein, which contributes to filopodia formation (Krugmann et al., 2001). However, previous studies with deletion mutants of IRSp53 lacking the SH3 domain in melanoma and neuroblastoma cells showed that the protein promotes actin reorganization also without the SH3 domain (Govind et al., 2001; Nakagawa et al., 2003). In addition to I-BAR and SH3 domains, some splice variants of IRSp53 subfamily proteins have a WH2-like domain in their C-terminal end, which reminds the conventional WH2 domain (Lee et al., 2007). IRSp53 and IRTKS also have a tryptophan, tryptophan -domain binding motif (WWB) in between SH3 and WH2 domains. In addition, IRSp53 has the partial-Cdc42/Rac interactive binding motif (CRIB) in between I-BAR and SH3 domains (for review see Zhao et al., 2011).

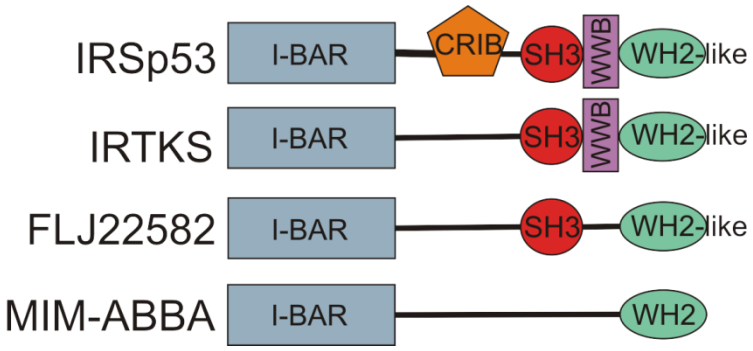

Figure 3. The domain structure of I-BAR domain proteins. The most important domains regarding protein function are shown. In addition to the common I-BAR domain, proteins of the IRSp53 subfamily contain a SH3 domain and a WH2-like domain in their C-terminal end, which is missing in most splice variants. IRSp53 and IRTKS also have a WWB in between these two domains. MIM-ABBA family proteins have a WH2 domain in their C-terminal end. The figure is modified from the reviews by Zhao et al. (2011) and Suetsugu et al. (2010).

IRSp53

IRSp53 was originally identified as a 58/53-kDa substrate of the insulin receptor tyrosine kinase and it is also referred to a brain-specific angiogenesis inhibitor 1-associated protein 2 (Yeh et al., 1996; Yamagishi et al., 2004). Since then, six splice variants of IRSp53 domain proteins have been found, which show differences in tissue distribution and differ in their C-termini implying to their distinct functions (Okamura-Oho et al., 2001; Lee et al., 2007). Two of the splice variants include proline-rich sequences, which have been shown to bind to post-synaptic density 95 and SH3 and multiple ankyrin repeat domains protein 1 forming a trimeric signalling complex during dendritic spine morphogenesis (Soltau et al., 2004). Another two isoforms have no extensions, which are functionally identifiable, while the remaining two splice variants present WH2-related extensions in their carboxy terminus (C-terminus). The WH2 domain of IRSp53 is different to the corresponding domain of MIM in the N-terminal end of the domain (Fig. 3). However, distinctions in this region did not affect binding of actin by IRSp53 as previously was proposed (Lee et al., 2007).

The I-BAR domain of IRSp53 binds to Rac and mediates binding of the CRIB domain to Cdc42. Rac and Cdc42 are the Rho family small G-proteins involved in lamellipodia and filopodia formation, respectively (Miki et al., 2000; Krugmann et al., 2001; Nakagawa et al., 2003). The binding of Cdc42 to IRSp53 enhances attachment of SH3 domain to the proline-rich region of mammalian enabled protein (Krugmann et al., 2001).

IRSp53 localizes on the plasma membrane by the I-BAR domain (Miki et al., 2000; Nakagawa et al., 2003; Suetsugu et al., 2006). The protein contributes to filopodium formation as observed by the extensive formation of filopodia when IRSp53 I-BAR domain was ectopically expressed in cultured cancer cells. (Yamagishi et al., 2004).

Choi et al. (2005) showed that overexpression or removal of IRSp53 expression by ribonucleic acid (RNA) interference altered spine morphology, density and size. In addition, a dominant-negative IRSp53 with mutated SH3 region and the proline-rich region of dominant-negative WAVE2 induced spines with decreased size and density. Based on these results, the SH3

domain of IRSp53 was suggested to play significant role in linking IRSp53 to downstream effectors of activated Rac1/Cdc42 during spine morphogenesis.

IRTKS

IRTKS gene encodes a 511 aa. long protein which has 39% identity to human IRSp53. The sequences of these proteins share high homology in the regions of the I-BAR domain, SH3 and WWB. However, conservation is significantly lower outside of these sites. The most evident difference in the structure of IRTKS when compared to IRSp53 is the lack of a partial CRIB motif in IRTKS (Fig 3.). IRTKS is widely distributed in tissues and has mainly been found from liver, bladder, heart, lung and testes in mice. Similarly to IRSp53, IRTKS has also been observed to function as an insulin receptor substrate (Millard et al., 2007).

Millard et al. (2007) showed with pulldown assays including glutathione S-transferase (GST)-tagged constitutively active and dominant negative mutants of Cdc42 that IRTKS is not able to bind to Cdc42. However, IRTKS can bind to Rac, which is due to the localization of Rac binding site within the conserved I-BAR domain. Therefore, IRTKS is proposed to be mainly mediating lamellipodia formation in migrating cells.

Some IRTKS and IRSp53 splice variants also contain a WH2-like domain in their C-terminus. However, the sequence of the C-terminal end is unique for IRTKS and has been shown to play an essential role in actin cluster formation. When the C-terminus of IRTKS was added to the full-length IRSp53 construct, it promoted the formation of actin clusters reminiscent of the ones formed by a full length IRTKS construct. In addition, expression of the IRTKS construct lacking the C-terminal WH2-like sequence showed filopodia-like extensions in cells, whereas actin clusters were absent (Millard et al., 2007).

Interestingly, the previous studies have shown that in enterohemorrhagic *Escherichia coli* (*E. coli)* infected cells, IRSp53 and/or IRTKS interact with bacterial translocated intimin receptor (Tir) and enterohemorrhagic *E. coli* secreted protein FU (EspFU) in pedestal formation (Vingadassalom et al., 2009). Pedestals are actin filament-filled pseudopods, which form

beneath the sites of bacterial attachment in the epithelium of the intestine. Tir interacts with intimin in the bacterial outer membrane resulting in Tir clustering, while EspFU mediates actin polymerization by binding to and activating N-WASP. Both of these events are required for pedestal formation (Liu et al., 2002; Campellone et al., 2004). Vingdassalom et al. (2009) showed that IRTKS was able to bind to Tir and EspFU *in vitro* and it was recruited to enterohemorrhagic *E. coli* interaction sites *in vivo*. Small interfering RNA experiments showed that only IRTKS was essential for the pedestal formation and that the IRSp53 depletion did not affect it. However, Weiss et al. (2009) contrasted these results by providing evidence that also IRSp53 is involved in pedestal formation.

FLJ22528

FLJ22528 is also referred as brain-specific angiogenesis inhibitor 1-associated protein 2-like protein 2 encoding a 529 aa. long protein (http://www.ncbi.nlm.nih.gov/protein/NP_079321.3, 24.5.2011). In addition to the general domain structure, much is still not known about FLJ22528. It belongs to IRSp53 subfamily and has the I-BAR domain and a C-terminal SH3 domain, whereas it is lacking the partial CRIB motif and WWB (Yamagishi et al., 2004).

1.8.2 The MIM/ABBA subfamily

MIM domain subfamily comprises genes *MIM* and *ABBA* encoding the corresponding proteins MIM and ABBA. Both proteins are accompanied with an I-BAR domain including the actin and Rac interaction sites. The I-BAR domain is followed by a serine-rich area, where three potential tyrosine phophorylation motifs are located, a proline-rich area comprising of WWB and SH3 domain interaction sites and a WH2 domain (Machesky and Johnston, 2007).

MIM

MIM was originally considered as a tumor suppressor as it was found from non-metastatic bladder cancer, while it was absent in metastatic cells. Therefore MIM was named as missing-in-metastasis (Lee et al., 2002). Mattila et al. (2003) observed MIM messenger RNA (mRNA) expression in the heart, differentiating postmitotic neurons and skeletal muscle in developing

mice. In adult mice MIM was mainly expressed in liver, the Purkinje cells of the cerebellum and the outer medullary zone of kidney.

Two MIM I-BAR domain splice variants have been found in vertebrates differing from each other by a four-amino-acid insertion. The splice variants are referred to as MIM/I-BAR domain-long and MIM/I-BAR domain-short. Interestingly, only MIM/I-BAR domain-short has been shown to interact with Rac. However this difference in binding did not affect filopodia formation in cells and hence, the roles of the two alternatively spliced forms of the I-BAR domain of MIM are still elusive (Mattila et al., 2007). In addition, Mattila et al. (2007) showed that the domain of MIM localized in between the plasma membrane and the bundles of F-actin when expressed in cells, and that the association of the domain with $PI(4,5)P_2$-rich membranes was required for filopodia formation.

In addition to its membrane binding activity, MIM promotes cortactin-mediated actin polymerization *in vitro* (Lin et al., 2005). MIM has also been identified as a G-actin-binding protein that inhibits F-actin nucleation and the nucleotide exchange on G-actin. Point mutation studies have shown that the G-actin binding site of MIM resides in the C-terminal end of the protein (Mattila et al., 2003).

Interestingly, Saarikangas et al. (2011) showed that MIM is essential for maintaining kidney epithelia integrity in mice due to its capability to interact with actin and plasma membrane in intercellular junctions.

ABBA

ABBA gene encodes for a 747 aa. long protein referred to as ABBA (Yamagishi et al., 2004). Similarly to MIM, ABBA contains a C-terminal WH2 domain and has a convex-shaped membrane binding motif (Yamagishi et al., 2004; Zheng et al., 2010). ABBA is strongly expressed in radial glial cells of the developing central nervous system in mice (Saarikangas et al., 2008).

ABBA binds to G-actin via the WH2 domain, and it has a higher affinity to ATP-G-actin than to ADP-G-actin suggesting that it is involved in actin filament assembly. However, interfering the G-actin binding to WH2 domain of I-BAR domain did not affect the cellular function of ABBA, proposing that actin-binding is not the main physiological function of this protein (Saarikangas et al., 2008). Additionally, ABBA also interacts with Rac to induce membrane deformation (Zheng et al., 2010).

ABBA I-BAR domain binds to PI(4,5)P_2-rich membranes and induces strong membrane tubulation *in vitro*. Membrane binding activity was shown by a cosedimentation assay, where ~90% of ABBA I-BAR domain bound to vesicles in the presence of PI(4,5)P_2. The ability of ABBA I-BAR domain to induce vesicle clustering and membrane tubulation was confirmed by mixing lipid vesicles with ABBA I-BAR domain and observing the samples by electron microscopy (Saarikangas et al., 2008).

Depletion of ABBA in radial-glia like C6-R cells led to reduced speed in membrane extension and ruffle formation at the leading edge during cell elongation. Endogenous ABBA was found localized in between the actin cytoskeleton and the cell membrane by confocal microscopy, which further confirms the significance of ABBA in the formation of membrane protrusions. In addition, massive formation of microspikes was observed during ectopic expression of ABBA I-BAR domain and this observation correlated well with the *in vitro* tubulation activity of the domain (Saarikangas et al., 2008).

Aims of the study

This study focused on determining association of I-BAR domain proteins with invadopodia in a highly invasive breast cancer cell line MDA-MB-231. In addition, I studied if the invasive glioblastoma cell line SNB-19 utilizes similar mechanism to drive its cell invasion. The composition of ECM in the central nervous system differs from other tissues and although highly invasive, gliomas are non-metastatic. Therefore, I wanted to analyse if gliomas use similar invasion strategy as metastatic breast cancer cells. The main focus of this study was to analyze the role of I-BAR domain proteins in invasive processes of cancer cells. Hence, I studied their expression in invasive breast cancer and glioma cell lines and examined their localization to invasive structures.

The specific aims of the study:

1. Exploring the I-BAR domain protein expression at mRNA and protein level in breast cancer cell line MDA-MB-231 and in glioma cell line SNB-19.

2. To establish an ECM degradation assay for studying localization of I-BAR domain proteins in invadopodia. Both endogenous and ectopically expressed I-BAR domain proteins were involved in localization studies. The intensity profiles for each I-BAR domain protein were measured to determine the accumulation levels of the I-BAR domain proteins in invadopodia.

3. To investigate if invadopodia can be detected in three dimensional (3D) environment. For this the localization of ABBA in cells inside 3D matrix was studied with confocal microscopy.

Materials and methods

1.9 Reverse transcription polymerase chain reaction (RT-PCR)

RT-PCR is a method, where RNA is converted into DNA by reverse transcription and polymerase chain reaction. First, reverse transcriptase enzyme is used to produce a double stranded RNA-complementary DNA (cDNA) hybrid, where cDNA corresponds to the gene of interest without the introns. Next, the hybrid is denatured, RNA is removed and the single-stranded cDNA is used for polymerase chain reaction (PCR) amplification to obtain extensive amount of double-stranded DNA.

1.9.1 RNA isolation

MDA-MB-231 and SNB-19 cells were treated with TRIZOL-reagent (Invitrogen) in 10 cm diameter plates. Cells were lysed with 6 ml of Trizol and mixed by passing the cell lysate several times through a pipette. To obtain the complete dissociation of the nucleoprotein complexes the mixture was incubated for 5 minutes at room temperature (RT). 1,2 ml of chloroform (Sigma-Aldrich) was added to the mixture, which was shaked vigorously for 15 seconds followed by incubation for 3 minutes at RT. The solution was centrifuged at 1 150 x gravitational force (g) for 15 minutes at +4 ^{o}C. After addition of chloroform and the subsequent centrifugation the solution separated into an aqueous phase containing the RNA, an interphase and an organic phase. RNA was precipitated from the aqueous phase by adding 3 ml isopropyl alcohol (Sigma-Aldrich) to the separated aqueous phase and incubating the solution for 10 minutes at RT. After incubation the samples were centrifuged at 1 150 x g for 10 minutes at +4 ^{o}C. The pellet was washed once with 6 ml of 75 % ethanol, after which the sample was mixed by vortex and subsequently centrifuged at 7 500 x g for 5 minutes at +4 ^{o}C. The RNA pellet was air-dried for ~10 minutes and redissolved in MilliQ-H_20. The dissolved RNA was incubated for 10 minutes at +56 ^{o}C and subsequently stored at -70 ^{o}C.

1.9.2 cDNA synthesis

First-strand cDNA was synthesized from the RNA isolated from MDA-MB-231 and SNB-19 cells by SuperScript II Reverse Transcriptase enzyme. First, total RNA from the previous step was combined with OligodT (Fermentas) and nucleotides. RNA concentration in the reaction was 1 µg, while OligodT was used with the final concentration of 8,3 x 10^{-6} µmol/µl. In addition, each nucleotide was used with the final concentration of 8,3 x 10^{-4} µmol/µl and the reaction mix was filled to its final volume with MilliQ-H_20. Second, the reaction mixture was heated at +65 ^oC for 5 minutes and subsequently chilled on ice. The contents of the reaction mixture were collected by brief centrifugation at 16 060 x g, after which First-strand buffer (Invitrogen), DTT (Invitrogen) and RNaseOUT Recombinant Ribonuclease Inhibitor (Invitrogen) were added to the mixture. The First-strand buffer was added to 1-fold, the final concentration of DTT in the reaction mixture was 0,01 M, whereas the final enzymatic activity of the RNaseOUT was 0,11 unit (U)/µl. The function of the RNAseOUT enzyme was to protect mRNA and improve total cDNA yields.

Third, the reaction mixture was gently mixed and incubated at +42 ^oC for 2 minutes. SuperScript II Reverse Transcriptase enzyme (Invitrogen) was added to the reaction mixture with the final enzymatic activity of 10 U/µl. The reaction mixture was incubated at +42 ^oC for ~50 minutes and subsequently the enzymatic activity of SuperScript II Reverse Transcriptase enzyme was inhibited by heating the mixture at +70 ^oC for ~15 minutes.

RNA complementary to the cDNA was removed with *E. coli* RNase H (Invitrogen), which was added to the reaction mix with the final concentration of 0,15 U/µl. After the addition of the enzyme, the mixture was incubated at +37 ^oC for ~20 minutes.

1.9.3 PCR from the total RNA

Primer BLAST (NCBI) was used for designing the primers, which were specific for each human I-BAR mRNA sequence and spanned exon-exon junctions. The sequence for the ABBA primer pair was 5'-CAGTGCCAAGGGTGGCGGAG-3' and 5'-

CTCACCGTGCTTGGCTGCGA-3', for MIM 5'-ACACGTGGTGGGACCAGGGA-3' and 5'-TGGTGGTGCTGGGGGAAGAGG-3', for IRSp53 5'-GCGCGGTCCATGAGCAGGAAT-3' and 5'-GGCAGGAGAAGCAGCAGGGC-3', for IRTKS 5'-ACGTGTCCAAGGCGAGGGGT-3' and 5'-CGGAGAGGCCCGGGAGAGTC-3', for FLJ22582 5'-TGCGTGCCTTCCACGCTCTG-3' and 5'-CAGCACGCGGTTCTGGAGCA-3' and for the actin control 5'-CTTTTGCGTCGCCAGCCGAG-3' and 5'-TGACCT TGGCCAGGGGTGCT-3'. All primers were obtained from Oligomer. Five separate reactions were prepared containing distinct primer pairs, which were planned to multiply a fragment of 400-600 bp from the 5´ region of the corresponding mRNA. The sixth reaction was performed with an actin control primer pair. 2 µg of cDNA from the previous reaction was obtained for each reaction, where each primer was used with the final concentration of 0,5 µM/µl and the remaining reaction volume was filled with MilliQ-H_20. All reactions were performed using GoTaq Green Master Mix (Promega). The PCR amplification program was the following: 2 minutes initial denaturing at +95 ^oC, 35 cycles of [40 seconds at +95 ^oC (denaturing), 40 seconds at +55 ^oC (annealing), 50 seconds at +72 ^oC (extension)] and final extension at +72 ^oC for 5 minutes. The reaction products were analyzed on 1,2 % agarose gel with 1 kilo base (kb) and 50 base pairs DNA ladders (GeneRuler™) with the voltage of 60 V for 2 hours to ensure the correct sizes of amplified fragments.

1.10 Western blot

The Western blot method is a well-known analytical method for detecting proteins in a tissue extract. The samples containing specific denaturated proteins are separated by gel electrophoresis by their molecular weights and transferred to a nitrosellulose membrane to be probed with antibodies specific to the protein of interest. Also native proteins can be used for the assay in which case the separation is based on the 3D structural properties of the protein. In this study, the proteins of the tissue extract were denatured before their separation with sodium dodecyl sulfate polyacrylamide gel electrophoresis.

MDA-MB-231 and SNB-19 cells were cultured on 10 cm diameter tissue plates for 24 hours and washed twice with 1 x phosphate-buffered saline (PBS) (8 g/l NaCl, 0,2 g/l KCl, 1,4 g/l Na_2HPO_4 x $2H_2O$, 0,2 g/l KH_2PO_4). Cells were scraped from the plate and centrifuged at 250 g by a Falcon centrifuge 5810R (Eppendorf) for 5 minutes at +4 ^oC. The pellet was resuspended in lysis buffer containing PBS, 1 % Triton X-100 (Sigma-Aldrich), 0.2 mM sodium orthovanadate (Sigma-Aldrich) and a Complete Protease Inhibitor Cocktail Tablet (Roche). The resuspension was mixed with phenylmethylsulfonyl fluoride (Sigma-Aldrich) to the final concentration of 0.2 mM. The mixture was incubated for 30 minutes at RT with occasional mixing. The cells were lysed by sonication using 5 x 5 seconds bursts on ice and the pellet was collected by centrifugation at 16 060 x g for 5 minutes with Biofuge Pico (Heraeus). The supernatant was stored at -70 ^oC. The protein concentration for Western blotting was determined by Bradford protein assay, where the standard curve was made from bovine serum albumin (BSA, Sigma-Aldrich). Total of 40 µg of protein lysate was used for 10 % sodium dodecyl sulfate polyacrylamide gel electrophoresis and the molecular weights were determined by Precision Plus Protein Dual Color Standards (BIORAD). The samples were concentrated on the upper gel (3,75 %) at 80 V for 15 minutes after which the separation of the samples was performed on the lower gel (13,5 %) at 150 V for ~1 hour. The proteins were blotted on a nitrocellulose membrane at 100 V for 1 hour and subsequently the membranes were incubated in 5 % non-fat dried milk in 1 x Tris-buffered saline (TBS) (3 g/l Tris, 8 g/l NaCl, 0,2 g/l KCl, pH 7,4) -Tween containing 0,1 % Tween (Sigma-Aldrich) at +37 ^oC for 60 minutes in shaking. All primary and secondary antibody dilutions were made in the buffer mentioned above. The membranes were treated separately with anti-IRTKS (Atlas Antibodies) and anti-IRSp53 (Atlas Antibodies) antibodies generated in rabbits with the 1:250 dilutions. Anti-ABBA-rabbit (Saarikangas et. al 2008) was used with the dilution of 1:500. Mouse-derived anti-α-tubulin (Sigma-Aldrich) was used as a control with the dilution of 1:1000. The membranes were incubated in primary antibodies at +4 ^oC overnight, shaking. The membranes were washed for 3 x 10 minutes with TBS-Tween and incubated in secondary antibody for 1 hour at RT in the dark and shaking. The secondary antibody for the samples was anti-rabbit horse radish peroxidase (Finnzymes) in dilution 1:2000 and for the control anti-mouse horse radish peroxidase (Sigma-Aldrich) in 1:2000 was used. The membranes were subsequently

washed for 3 x 10 minutes with TBS-Tween at RT. After the last TBS-Tween treatment the membrane was placed on a parafilm and dried with a paper towel. The detection reagent mixture containing Western Lightning Plus ECL:Oxidizing reagent Plus and Enhanced Luminol Reagent Plus (PerkinElmer) in 1:1 ratio was added on the membranes. Then, the membranes were incubated for 60 seconds, the detection reagent mixture was removed and the membranes were placed separately in plastic bags for detection. Chemiluminescence detection was performed by LAS-3000 CCD-camera (Fujifilm) with the automatic exposure and super sensitivity. In addition, the membrane and the standard markers were visualized with 1/60 seconds exposure time and standard sensitivity.

1.11 Cloning IRTKS-cDNA into a pCherry-N1 plasmid

1.11.1 PCR amplification of IRTKS insert

In this study cDNA corresponding to full-length IRTKS sequence was multiplied with PCR. The cDNA template was purchased from Origene and the primers used for the PCR were 5'-GCG CTC GAG ATG TCC CGG GGG CCC GAG GAG G-3' and 5'-GGC GGA TCC GCT CGA ATG ATG GGT GCC GAG CGA-3'. The PCR amplification program was: 2 minutes initial denaturing at +95 ^{o}C, 35 cycles of [40 seconds at +95 ^{o}C (denaturing), 40 seconds at +68 ^{o}C (annealing), 1 minute at +72 ^{o}C (extension)] and final extension at +72 ^{o}C for 5 minutes. Due to problems in obtaining pure product, the PCR reaction conditions were optimized by running the reaction in several annealing temperatures (+58 ^{o}C, +62 ^{o}C, +66 ^{o}C and +68 ^{o}C) where the highest temperature resulted in the purest product. This was observed as the reaction products were analyzed on 1 % agarose gels with the voltage of 80 V to ensure the correct size of the amplified fragment. The DNA fragment was excised from the gel from two separate wells, which were combined to maximize the quantity of the product, purified with the QlAquick PCR Purification Kit (Qiagen) and eluted in MQ-H_20.

1.11.2 Digestion and ligation

Digestion is a method, where double stranded DNA is cut by restriction enzymes. These enzymes recognice a specific sequence and cleave the DNA by making breaks to the phosphate backbone of the double helix. The multiplied ITRKS-cDNA insert and an empty Cherry-N1 plasmid (Clontech Laboratories) were double-digested with BamHI and XhoI restriction enzymes (Fermentas) to create ends where the insert can attach in a correct orientation. Both the insert and the plasmid were digested at +37 ^{o}C for 3 hours. The reaction products were analyzed by agarose gel electrophoresis on 1 % gel for about 1 hour 30 minutes. The products were excised from the agarose gel and purified with PCR clean-up Gel extraction kit (Macherey Nagel).

In a ligation reaction, two linear DNA fragments are joined together by introducing a covalent phophodiester bond between them. First, the Cherry plasmid and the IRTKS insert were ligated with T4 ligase (New England Biolabs) in a molar ratio of 1:3. The enzyme was used with the activity of 0,7 U/µl, while T4 ligase buffer (New England Biolabs) was added to the reaction in 1 x dilution and the reaction mixture was incubated at +16 ^{o}C overnight. Subsequently, the ligation reaction was introduced into bacteria to promote multiplication of the plasmid. 10 µl of ligation reaction was introduced into transformation competent *E. coli* DH5α cells by heat shock. Next, the bacterial cells were defrosted on ice for 20 minutes, after which the plasmid DNA from the ligation reaction was added to the cells and the mixture was incubated for 5 minutes on ice. Cells were heated at +42 ^{o}C for 1 minute, incubated on ice for 1 minute and suspended to Luria-Bertani (LB) medium to recover from the heat shock. Transformed cells were incubated at +37 ^{o}C in shaking and plated on LB medium plates containing 100 µg/ml of kanamycin. The transformation mixture was added on the plate with 10 x dilution and incubated at +37 ^{o}C overnight. The following day 2 colonies were selected and inoculated into LB medium containing 100 µg/ml kanamycin. Next, the transformed bacteria were cultured in shaking at +37 ^{o}C overnight and collected by centrifuging them in a Falcon centrifuge 5810R (Eppendorf) at 3300 x g for 5 minutes. Finally, the plasmid DNA was isolated and purified using GenElute Plasmid Miniprep Kit (Sigma-Aldrich) and eluted in MQ-H_2O.

1.11.3 Test digestion

One µg of purified IRTKS-Cherry construct was used for test digestion with BamHI and XhoI restriction enzymes (Fermentas), which were added to the reaction mix with the final enzymatic activity of 0,25 U/µl. Buffer 3 and BSA (New England Biolabs) were used in 1-fold concentration for the digestion reaction mix, which was filled with MilliQ-H_20 to achieve the final reaction volume. The reaction was incubated at +37 ^oC for an hour and the digestion products were analyzed by agarose gel electrophoresis on a 1 % agarose gel with the voltage of 80 V. 1 kb DNA ladder (Gene Ruler) was used for analyzing the size of the product. One of the colonies was sequenced in DNA sequencing and Genomics laboratory, University of Helsinki to ensure the correct sequence.

1.12 Sub-cloning IRTKS into a green fluorescent protein (GFP)-N1 plasmid

The sequenced IRTKS-Cherry plasmid was digested with FastDigest BamHI and XhoI enzymes (Fermentas) following the manufacturer's instructions for the enzymes. Four µg of IRTKS-Cherry plasmid was used for the reaction and the reaction mixture was incubated at +37 ^oC for 15 minutes. The digestion products were analyzed by agarose gel electrophoresis on 1 % gel run at 95 V. The products were excised from the agarose gel and purified with PCR clean-up Gel extraction kit (Macherey Nagel). The ligation, transformation and purification of IRTKS-GFP-N1 were performed as previously, except for that the transformation mixture was added on the LB medium –plates containing kanamycin with both 1 x and 10 x dilution. In addition, the GFP-N1 vector used for the ligation was treated with Calf Intestinal Alkaline Phosphatase (New England Biolabs) with the final enzymatic activity of 0,2 U/µl to inhibit plasmid self ligation by removal of the 5' phosphate group's from the plasmid DNA. After Calf Intestinal Alkaline Phosphatase had been added to the reaction mixture it was incubated at +37 ^oC for 30 minutes. Upon the day following transformation, 5 bacterial colonies were picked from the plates, inoculated in LB overnight and the plasmid was extracted by GenElute

Plasmid Miniprep Kit (Sigma-Aldrich). The products were analyzed by conducting a test digestion and subsequent agarose gel electrophoresis.

1.12.1 Maxiprep

To obtain large quantities of IRTKS pCherry-N1 and pGFP-N1 plasmids, they were transformed into *E. coli* DH5α cells and cultured in a small scale as described previously. Five ml of the inoculation media was added to 150 ml and incubated for 16 hours in shaking. The bacterial cells were harvested by centrifuging them in a Falcon centrifuge 5810R (Eppendorf) at 3 300 x g for 30 minutes at +4 ^{o}C and the supernatant was removed to be further processed with QlAfilter Plasmid Maxi Kit (Qiagen). The instructions in the manual were followed with minor exceptions. After addition of chilled Buffer P3, the lysate was incubated for 20 minutes at RT, poured into a barrel of QlAfilter Cartridge and incubated for 10 minutes at RT without subsequent centrifugations. RC 5C high speed centrifuge (Sorvall Instruments) with Sorvall SS-34 rotor was used to separate precipitated DNA from the elution buffer at the speed of 11 369,5 x g. After washing of the pellet with 70 % ethanol the resuspension was divided into aliquots. The pellet was concentrated by centrifugation for 5 minutes at 16 060 x g with Biofuge Pico (Heraeus). The aliquots were combined by three washes of 70 % ethanol where the first aliquot was washed with and resuspended to ethanol and the resulting resuspension was transferred to the next aliquot. After each ethanol wash the resuspension was pelleted by centrifugation at 16 060 x g for 5 minutes. The final pellet was vacuum-dried in Eppendorf vacuum for 10 minutes. The program used for the drying was Desiccator D-AL.

1.13 Purification of anti-ABBA antibody with affinity columns

Serum was obtained from whole blood of a rabbit immunized with a protein fragment containing aa. 274-683 of mouse ABBA. All columns used for the anti-ABBA antibody purification were prepared by PhD Juha Saarikangas, Institute of Biotechnology, University of Helsinki. Columns were prepared by covalently immobilizing GST, MIM (aa. 297-727) or ABBA (aa. 274-683) fragments to the column and each column was washed twice with PBS

before addition of serum. Serum was added to a GST-column with PBS to remove impurities in serum that bind to the column resin. Serum in PBS was mixed with resin until the mixture was homogeneous and incubated at +4 ^{o}C for ~30 minutes in rotation. Subsequently, the mixture in the column was incubated at RT before the flow-through was collected. The flow through was added to the MIM-column following the same procedure as with GST-column. This step was essential as the ABBA and MIM are highly homologous proteins at the aa. sequence level. By incubating the serum in MIM column, the antibodies recognizing shared epitopes in MIM and ABBA should be removed. The flow through was collected and directly added to an ABBA column. The column was washed three times with PBS before elution of anti-ABBA antibody with fresh 100 mM glycine (pH 2,7) that was prepared from glycine powder (Sigma-Aldrich). Five 1 ml fractions were collected and analyzed with Brilliant Blue R 250 (Sigma-Aldrich) to detect fractions containing highest amount of antibodies. Three fractions including anti-ABBA antibody were pooled and concentrated with Amicon Ultra Centrifugal Filter (Millipore) to a total volume of 500 µl at +4 ^{o}C. Finally, Na-azide to 0.03 % and BSA (Sigma-Aldrich) to 1 mg/ml were added to the antibody solution, which was stored at +4 ^{o}C. The specificity of the affinity purified antibody was tested by Western blotting.

1.14 Cell culture

Human breast cancer cell line MDA-MB-231 was originally obtained from PhD Jacco Van Rheenen (Hubrecht Institute, The Netherlands) and cultured in Dulbecco's Modified Eagle Medium (DMEM) (Sigma-Aldrich) supplemented with 10 % fecal bovine serum (Gibco) and antibiotics (20 mM L-glutamine, 1000 U penicillin, 1 mg streptomycin, Sigma-Aldrich) at +37 ^{o}C 5% CO_2. For the invadopodia assay the amount of fecal bovine serum in DMEM was increased from 10 to 15 %. Cells were split on a regular basis and used at ~70 % confluence

1.15 ECM degradation assay

1.15.1 Coating coverslips with fluorescent gelatin matrix

Coverslips were prepared using an ECM degradation assay protocol described by Artym et al. (2009), with the exception that the coverslips were autoclaved instead of flaming. First, coverslips were washed with 20 % nitric acid for 30 minutes and gently swirled during the acid-wash. Next, the coverslips were washed for ~2 hours with deionized water, which was changed frequently. The coverslips were autoclaved overnight, after which they were placed on the wells of a 12-well tissue culture plate (Falcon). The coverslips were coated with prechilled 50 µg/ml poly-L-lysine (Sigma-Aldrich) for 20 minutes, washed three times with PBS and crosslinked with 0,5 % of freshly-made glutaraldehyde solution (Sigma-Aldrich) for 15 minutes.

Alexa Fluor 568 Monoclonal Antibody Labeling Kit (Molecular Probes®) was used for labeling 0,2 % gelatin from porcine skin, type A (Sigma-Aldrich). First, gelatin was weighted and dissolved into PBS, followed by heating at +37 ^{o}C for 30 minutes. Gelatin solution was filtered through a syringe filter membrane with 0,22 µm pore size. 500 µl of 0,2 % gelatin was heated at +37 ^{o}C for ~10 minutes, while in the meantime the Alexa Fluor 568 dye (Molecular Probes®) was equilibrated to RT. Sodium bicarbonate (Molecular Probes®) was mixed with the preheated gelatin to achieve the final concentration of 0,09 µM and combined with Alexa Fluor 568 antibody (Molecular Probes®). The solution was inverted for three times and incubated for 1 hour in the dark at RT and on shaking. Labeled gelatin-Alexa Fluor 568 and the free dye were separated by gel filtration. The gel filtration column was prepared for this by placing a spin column provided by the kit in a glass tube. The purification resin provided by the manufacturer was stirred, 1 ml of resin was added into the column and it was allowed to settle for a few minutes. More resin was added until the bed volume was ~1,5 ml. By creating pressure to the upper end of the column the buffer removal from the column was initiated, while the rest of the buffer was drained by gravity. The spin column was placed into a provided collection tube and centrifuged for three minutes at 1 100 x g, after which the buffer was discarded. After 1 hour incubation, the labeling solution was added dropwise to the

column and allowed to absorb into the resin for few minutes. Finally, the column was placed into the empty collection tube and centrifuged for 5 minutes at 1 100 x g. The labeled fraction was stored at +4 ^{o}C and used in the next step.

0,2 % unlabeled gelatin and labeled gelatin were mixed in 8:1 ratio and heated at +37 ^{o}C for ~10 minutes. The coverslips were washed three times with PBS and subsequently inverted on an 80 µl drop of Alexa Fluor 568-labeled gelatin for 10 minutes. The PBS washes were repeated and the coverslips were quenched with 5 mg/ml of freshly-made sodium borohydride (Sigma-Aldrich) for 15 minutes to prevent autofluorescence of the gelatin matrix. Gas bubbles that formed during the sodium borohydride treatment were removed by rocking the tissue culture plate. The coverslips were washed three times or more with PBS to remove all the bubbles. The coverslips were stored at +4 ^{o}C and used within six days.

1.15.2 Preparation of samples for fluorescent gelatin degradation assay

For the matrix degradation assay MDA-MB-231 cells were counted using hemocytometer, resuspended to a concentration of 2 x 10^5 and plated on fluorescent gelatin-coated coverslips. Cells were incubated at +37 ^{o}C for 3 hours, 6 hours, 24 hours or 48 hours with the intention to find the optimal length of incubation for invadopodia formation. 3 hour incubation was chosen for further experiments as in such time invadopodia were induced, while cells maintained their viability. After incubation, the cells were fixed and permeabilized following the protocol described by Artym et al. (2009). For labeling, the coverslips were removed from the wells of the tissue culture plate and inverted on the drops of 100 µl of Alexa Fluor 488-conjugated phalloidin (Molecular Probes®). Phalloidin was used with the dilution of 1:150 in Dulbecco PBS containing 0,2 % BSA, while it was incubated for 30 minutes at RT in the dark. The coverslips were washed three times with PBS, dipped into MQ-H_20 and attached to an objective glass. Sixty µl of Mowiol (Calbiochem)-Dabco (Sigma-Aldrich) per coverslip was used for mounting and the coverslips were left to polymerize overnight.

1.16 ECM degradation assay in 3D

1.16.1 Collagen matrix preparation

Six parts of chilled collagen (3 mg/ml pH 2, Sigma-Aldrich) was mixed with 4 parts of 2.5 x DMEM with 25 % fecal bovine serum. The pH was adjusted using pH paper to 7.2-7.6 with NaOH. Collagen solution was added on the coverslip and a sterile glass bead was added on top of the coverslip. Collagen was polymerized at +37 ^{o}C for 2 hours after which the beads were removed from the gel.

1.16.2 Sample preparation for 3D colocalization assay

Fresh MDA-MB-231 cells were thawn for the experiment, resuspended into DMEM with 10 % of fecal bovine serum and antibiotics and incubated overnight at +37 ^{o}C. Cells were trypsinated and counted by hemocytometer to achieve a total amount of 2 300 cells per sample. Cells were centrifuged at 500 g for 3 minutes and resuspeded to 100 µl of serum free DMEM (Sigma-Aldrich). Resuspeded cells were mixed with 10 µl of ECM (Sigma-Aldrich) per sample and the mixture was added on the holes formed at the centre of the collagen matrix. The matrix was incubated at +37 ^{o}C for 15 minutes to allow the mixture of cells and ECM to polymerize. Finally, cell culture media was added and the gel was incubated at +37 ^{o}C for ~23 hours after which they were fixed and stained as described in the following chapter.

1.16.3 Immunostaining

After 3 hour incubation, MDA-MB-231 cells were fixed and permeabilized as described previously by Artym et al. (2009). I-BAR domain proteins were labeled with either rabbit anti-IRSp53 (1:250) (Atlas-Antibodies), anti-IRTKS (1:50) (Atlas-Antibodies) or anti-ABBA (1:50) (Saarikangas et. al 2008) primary antibodies in MDA-MB-231 cells, while SNB-19 cells were immunostained with anti-ABBA (1:50) primary antibody. To confirm the formation of invadopodia in MDA-MB-231 cells, cortactin was labeled with mouse anti-cortactin (Millipore) (1:150). All primary and secondary antibodies were diluted in Dulbecco PBS containing 0,2 % BSA. In both cell types I-BAR domain proteins were labeled with the

primary antibody for ~1 hour at RT. Alexa Fluor 488 goat anti-rabbit antibody (Invitrogen) (1:250) was used as a secondary antibody for targeting I-BAR domain proteins, whereas F-actin was targeted with Alexa Fluor 647-conjugated phalloidin (1:150) (Molecular Probes®) in breast cancer and glioma cells. Mouse anti-cortactin was targeted with Alexa Fluor 488 goat anti-mouse secondary antibody (Molecular Probes®) (1:250). Cells were incubated with the secondary antibodies and phalloidin for 30 minutes at RT in the dark.

For 3D analysis, the collagen pads were fixed with 4 % paraformaldehyde for 30 minutes and washed twice with PBS. Cells were permeabilized with 0.2 % Triton-X-100 (Sigma-Aldrich) in PBS for 30 minutes and washed in Dulbecco containing 0,2 % BSA for 3 hours with the change of Dulbecco after one hour incubation. ABBA was labeled with rabbit anti-ABBA with 1:100 dilution and cortactin was targeted with anti-cortactin (Millipore) made in mouse with 1:150 dilution overnight at +4 ^{o}C, gently rocking. The anti-ABBA antibody was prepared as described above. Two control samples were not treated with primary antibodies. After primary antibody incubation the matrix was washed 3 x 15 minutes with Dulbecco containing 0.2 % BSA and the secondary antibodies goat anti-rabbit Alexa Fluor 647 (1:250) and goat anti-mouse Alexa Fluor 568 (1:400) (Molecular Probes®) were added on the cells. Alexa Fluor 488 phalloidin (Molecular Probes®) was used for F-actin labeling with 1:200 dilution. Cells were incubated with the secondary antibodies and phalloidin for 2 hours at RT. After incubation secondary antibodies and phalloidin were removed by washing the matrix for 3 x 15 minutes with Dulbecco containing 0.2 % BSA. The matrix was dipped into MQ-H_2O and mounted with Mowiol-Dabco on 1.5 mm thick coverslips (Thermo Scientific).

1.16.4 Transfection of cells

MDA-MB-231 cells were used at ~80 % confluence and plated on a 6-well plate (Falcon). The cells were incubated at +37 ^{o}C overnight and transfected the following day with 2 µg of plasmid DNA. The amount of DNA was chosen based on the preliminary experiments. The constructs used for transfection included full length murine *ABBA* and *MIM* and human *IRTKS* and *IRSp53*. All open reading frames were in pGFP-N1 vector (Clontech Laboratories). An empty GFP-N1 plasmid was transfected to the cells as a control.

Transfections were performed with Lipofectamine 2000 (Invitrogen), which was chosen as a result of comparative analysis of Lipofectamine and Fugene (Roche). In this preliminary experiment the efficiency of Lipofectamine to induce MDA-MB-231 cell transfection with an empty GFP-N1 plasmid was higher than the corresponding efficiency induced by Fugene. First, the plasmid DNA was diluted in 250 µl of DMEM without serum. Lipofectamine 2000 reagent was mixed gently, 5 µl of the reagent was diluted in 250 µl of DMEM without serum to obtain the final concentration of 0,02 µg/µl. The mixture was incubated for 5 minutes at RT, the diluted DNA was combined and gently mixed with diluted Lipofectamine 2000. The mixture was incubated for ~20 minutes at RT to form the DNA-Lipofectamine 2000 complexes. After the incubation, complexes were added to each well on a 6-well plate, DMEM with serum was added to obtain the total volume of 2 ml per well and the solution was mixed gently by rocking. Cells were incubated for 5 hours at +37 ^{o}C 5% CO_2 and media was changed. The cells were incubated overnight at +37 ^{o}C 5% CO_2 prior to fixation and usage for ECM degradation assay described above.

1.16.5 Microscopy and image analysis

The samples for degradation assay were examined with a 63 x objective of Carl Zeiss Axio Imager 2 microcope. The images were processed with Adobe Photoshop CS5 and the intensity profiles for F-actin, gelatin matrix, GFP tagged or endogenous I-BAR domain proteins for a single invadopodium were obtained from line scans of fluorescent images by Image Pro Plus 5.1. (Media Cybernetics Incorporation). Five cells expressing each GFP tagged or endogenous I-BAR domain protein were selected for the measurements. An invadopodium was determined as a decrease in the Alexa Fluor 568 signal representing the degradation site, while a concomitant increase in the phalloidin Alexa Fluor 647 signal corresponded to the F-actin dot.

The samples and the controls obtained from the 3D matrix degradation assay were visualized with Leica TCS SP5 DM5000 upright microscope with the HCX PL APO 63 x glycerol objective. The images were obtained by sequential scans and processed with Bitplane Imaris version 7.2.0.

Results

1.17 I-BAR gene expression analysis in glioma and breast cancer cells

A PCR-based non-quantitative assay was used to determine if the mRNAs of different I-BAR domain protein encoding genes are present in MDA-MB-231 and SNB-19 cells. Total RNAs were isolated from MDA-MB-231 and SNB-19 cells, converted into cDNAs, which were subsequently used as templates in a PCR reaction containing I-BAR gene specific primers. The PCR products were analysed by agarose gel electrophoresis. The results portrayed in Figure 4 indicate that fragments of expected size were amplified for ABBA, IRSp53 and IRTKS. In the case of both IRSp53 and IRTKS, the size of bands amplified from the different cells lines was slightly different, which could indicate differential slicing of these genes in the two cell lines (Fig. 4). Although this method is not quantitative, it was noted that the ABBA PCR reactions amplified a much lower amount of DNA in MDA-MB-231 cells than in SNB-19 cell line. Furthermore, MIM was very weakly amplified in both cell lines (Fig. 4), indicating either low expression levels or poorly functional primers. FLJ22582 was not detected on the gel indicating that it is not expressed in breast cancer and glioma cells (Fig. 4). Actin control showed a fragment of expected size (Fig. 4).

The results of the gene expression analysis indicate that ABBA, IRTKS, IRSp53 and MIM mRNA may participate in cellular processes in invasive cancer cells.

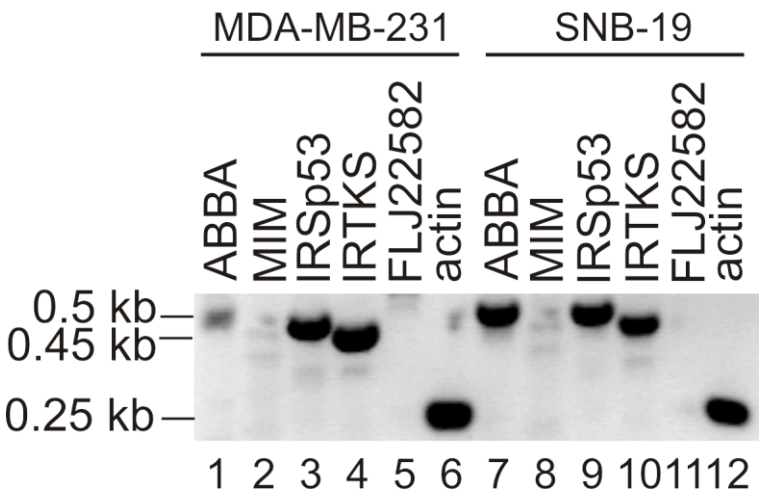

Figure 4. A RT-PCR gel showing the mRNA expression of each I-BAR domain protein fragment in breast cancer and glioma cells. The bands representing ABBA and IRSp53 fragments were 0.5 kb in size, whereas IRTKS fragment had a slightly shorter band which was 0.45 kb in size. ABBA was expressed at a lower level in MDA-MB-231 cells as compared with SNB-19 cells. The bands representing MIM expression were only weakly visible. FLJ22582 was absent from both cell lines, whereas actin control showed a band of expected size. Hence, all I-BAR domain proteins except for FLJ22582 were expressed at mRNA level in both cell lines.

1.18 I-BAR proteins are expressed in invasive breast cancer and glioma cells

To study whether the members of the I-BAR gene family are also expressed at the protein level in invasive cancer cells, a Western blot analysis was conducted with the available antibodies. Unfortunately, no functional antibody was available for MIM. The results portrayed in the Figure 5 show that IRSp53 had bands of different size in addition to the expected 50 kDa fragments in both cell lines indicating different isoforms of the protein. IRTKS showed bands, which had a size of 50 kDa and smaller in glioma cells, while ABBA predictably showed a band the size of ~100 kDa in both breast cancer and glioma cells. Moreover, the band indicating ABBA expression in SNB-19 cells was stronger than the corresponding band in MDA-MB-231 cells suggesting that ABBA is expressed at a higher level in glioma cells than in breast cancer cells (Fig. 5). Tubulin control showed bands of expected size in both cell lines (Fig. 5). These results suggested that ABBA, IRSp53 and IRTKS are expressed at protein level in glioma and breast cancer cells.

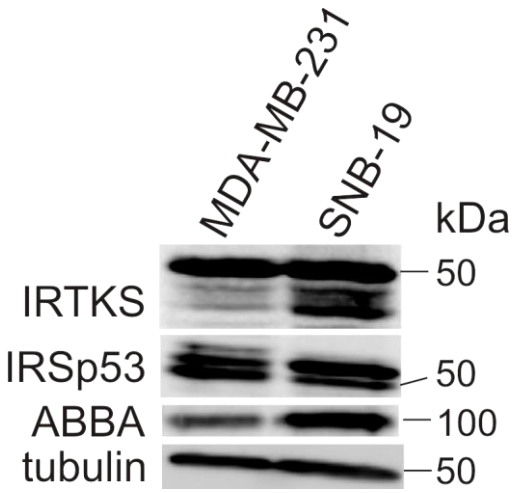

Figure 5. Western blot analysis of the expression of IRTKS, IRSp53 and ABBA I-BAR domain proteins in MDA-MB-231 and SNB-19 cells. IRSp53 had a band of 50 kDa in addition to few higher molecular weight bands which indicate splice variants. Extra bands were detected also for IRTKS in glioma cell line, while ABBA and tubulin control showed only bands of expected mobility. The results indicate that ABBA, IRSp53and IRTKS are expressed in MDA-MB-231 and SNB-19 cell lines and that ABBA expression is stronger in glioma cells than in breast cancer cells.

1.19 ECM degradation by invadopodia of MDA-MB-231 cells

The gelatin matrix degradation was observed by fluorescence microscopy in breast cancer and glioma cells. The cells were incubated on Alexa Fluor 568 labeled gelatin matrix for 3-5 hours in which time the cells formed invadopodia. Invadopodia were recognized by the degradation of gelatin matrix observed as dark spots on the matrix, which corresponded either with F-actin or cortactin spots.

F-actin and cortactin are both present in invadopodia (Artym et al., 2006) and hence, they represent invadopodia markes. The matrix degradation was observed as dark irregular spots on the fluorescent matrix, which colocalized with the bright F-actin spots in the cytosol (Fig. 6 A and B). Cortactin accumulated in the bright spots in the similar way with F-actin and localized to the degradation sites, further confirming that the matrix degradation was induced by invadopodia (Fig. 6 C and D).

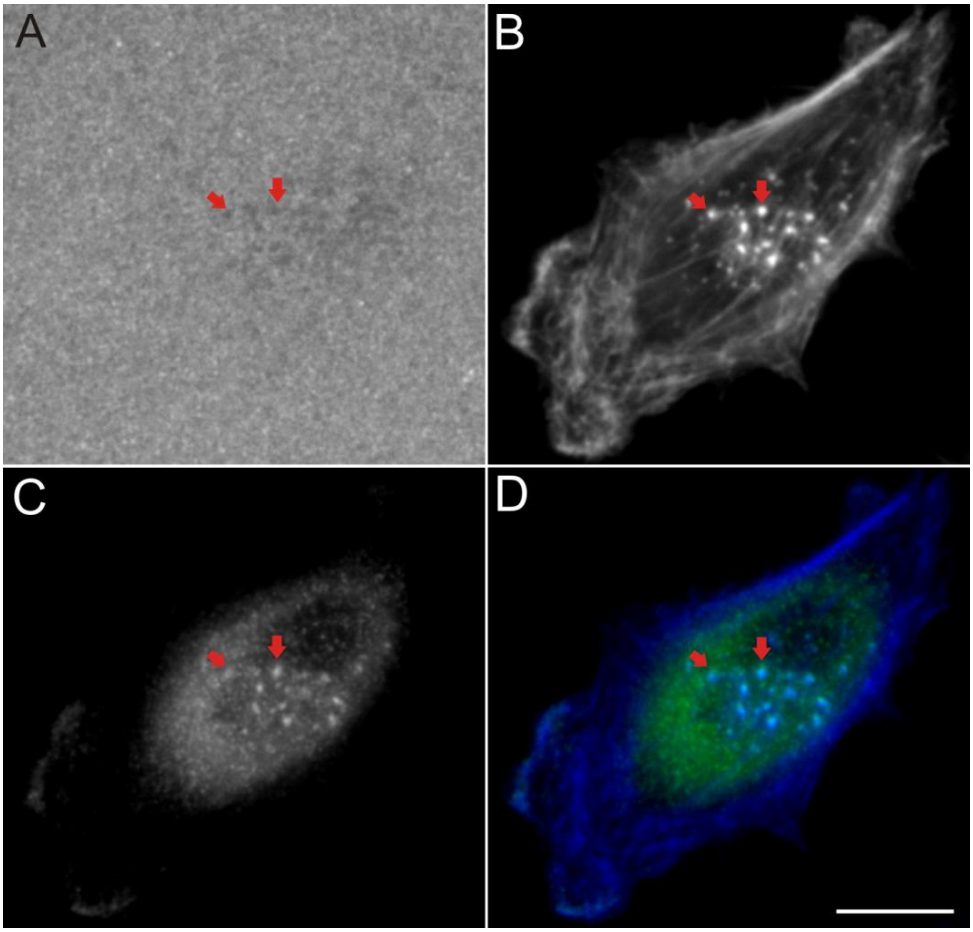

Figure 6. Degradation of fluorescent gelatin matrix by invadopodia of breast cancer MDA-MB-231 cells. The cells were incubated for 3 hours on top of the gelatin matrix. (A) Gelatin matrix proteolysis by invadopodia proteolysis was seen as dark spots in the fluorecent gelatin matrix. (B) In invadopodia, F-actin co-localized with the sites of degradation. (C) Endogenous cortactin labeled with anti-cortactin-mouse antibody, also localized to these spots (D) Channels from figures B and C were combined and the merging shows the colocalization of F-actin and cortactin at the same sites. Bar, 10 µm. The location of an invadopodium is shown by a red arrow. The images were acquired with Zeiss fluorescent microscope using a 63x/1.4 N. oil immersion objective.

1.20 Localization of endogenous I-BAR domain proteins to invadopodia

MDA-MB-231 cells were incubated on fluorescently-labeled gelatin matrix for 3 hours before fixation and immunostaining against endogenous ABBA, IRTKS or IRSp53. Invadopodia and F-actin dots were observed as previously described (Fig. 7 A and B). However, all antibody stainings showed widespread distribution in the cytosol and in the nucleus of the cell, hence there was no clear accumulation of antibody at the invadopodia sites (Fig. 7 C, 7 D and data not shown).

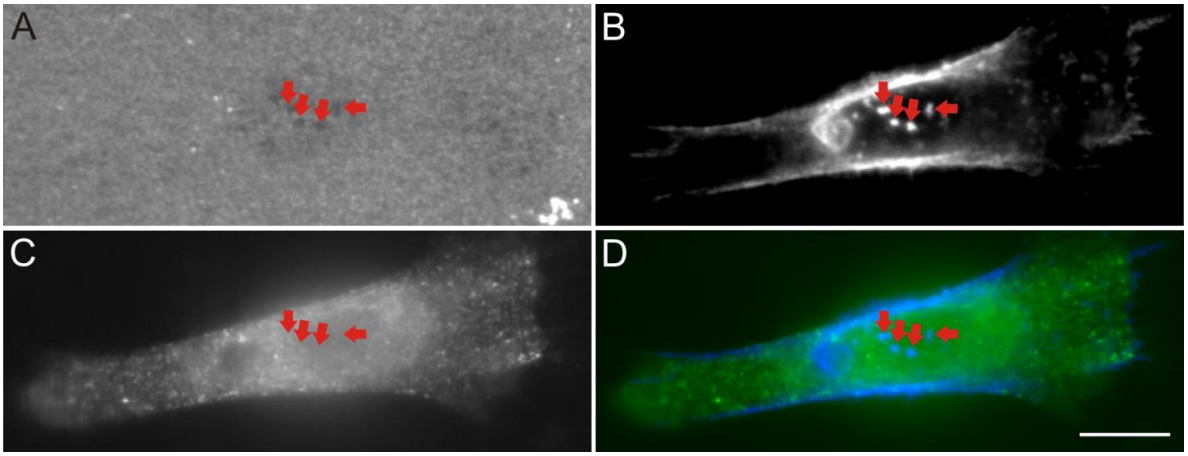

Figure 7. Gelatin matrix degradation by invadopodia of anti-ABBA-rabbit labeled MDA-MB-231 breast cancer cells. The cells were incubated on gelatin matrix for 3 hours. (A) Degradation of fluorescently labeled gelatin was seen as dark spots on the fluorescent matrix. (B) F-actin was labeled with phalloidin Alexa Fluor 647 and it localized to proteolytic sites on the matrix. (C) Endogenous ABBA was labeled with anti-ABBA antibody, which did not accumulate to invadopodia but was evenly distributed in the cell. (D) Channels from figures B and C were combined and the merging shows the diffuse localization of anti-ABBA antibody in the cell cytoplasm. Red arrows represent the sites of invadopodia. Bar, 10 µm. The images were acquired with Zeiss fluorescent microscope using a 63x/1.4 N. oil immersion objective.

1.21 ABBA in breast cancer cells on 3D collagen matrix

Although the localization of anti-ABBA antibody in two dimensional (2D) analysis was relatively homogeneous, it was interesting to see if the antibody would show accumulation in a distinct environment. Anti-ABBA antibody had previously been successfully used in immunocytochemical applications by Saarikangas et al. (2008) and therefore it was chosen for the 3D assay. In addition, I observed cell migration in the 3D experiments by confocal microscopy, which is a more sophisticated method and provides a more detailed view of the region of interest than regular wide-field immunofluorescence microscopy. However, the results portrayed in Figure 8 C show that similarly to 2D environment, ABBA was homogeneously distributed in MDA-MB-231 cells on 3D collagen matrix. Cortactin and F-actin staining were strong especially at the cell front (Fig. 8 A, B and D). In control cells antibody staining was not observed suggesting that the secondary antibody was specific to the primary antibody.

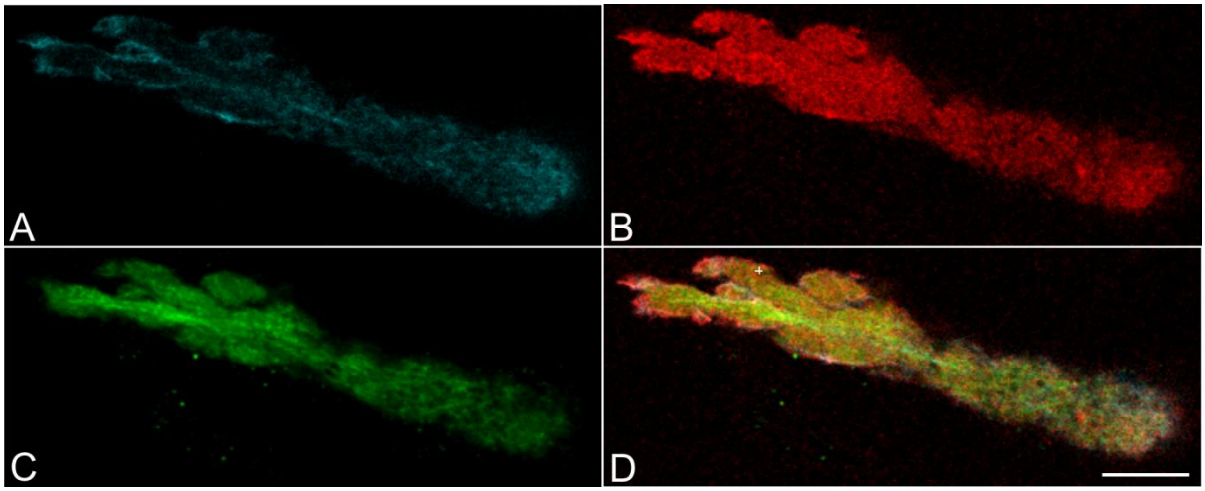

Figure 8. ABBA protein localization in MDA-MB-231 cells in 3D matrix. Breast cancer cells were incubated for 24 h in collagen matrix. (A) Phalloidin Alexa Fluor 488 was used for labeling actin filaments and it localized mainly at the tips of the cell. (B) Anti-cortactin mouse antibody was used for labeling endogenous cortactin in cells and the antibody showed a strong staining especially at the cell front. (C) Endogenous ABBA was labeled with anti-ABBA-rabbit antibody, which was widespread in the cell. (D) The merge picture was obtained by combining all three channels (A-C) showing the distribution of labeled proteins in the cell. Bar, 10 µm. The images were acquired with confocal microscopy using a 63x/1.4 N. glycerol objective.

1.22 Localization of ectopically expressed I-BAR domain proteins in breast cancer cells

Full-length MIM, ABBA, IRTKS and IRSp53 I-BAR domain proteins were expressed in MDA-MB-231 cells as fused to a fluorescent GFP-N1 plasmid.

Breast cancer cells were transfected with the GFP-tagged full-length I-BAR domain protein construct (I-BAR-GFP) or with an empty GFP-N1 plasmid, which was used as a negative control. In GFP-N1 transfected control cells the matrix degradation was observed as dark dots on the fluorescent matrix and it corresponded well with the bright F-actin dots (Fig. 9 A and B). In all control cells the GFP signal was highly diffuse showing no accumulation at the sites of invadopodia or F-actin (Fig. 9 C).

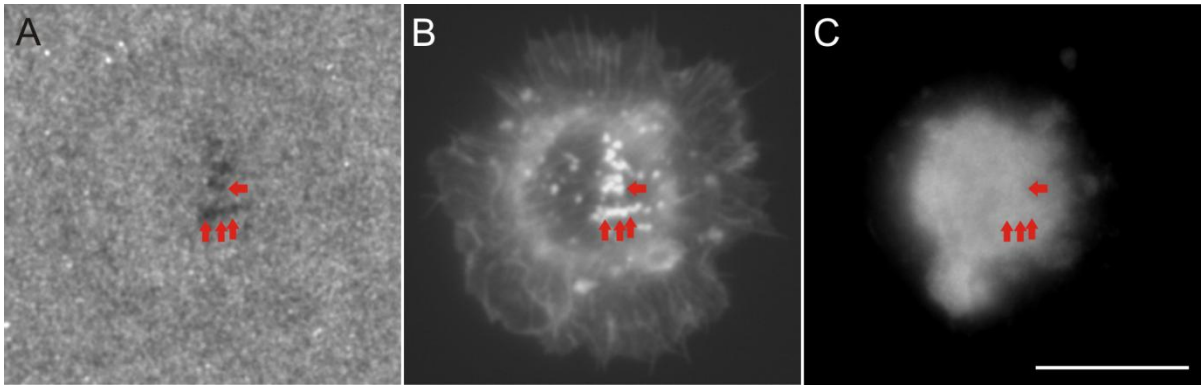

Figure 9. The proteolytic degradation of matrix by invadopodia of GFP-N1 transfected MDA-MB231 control cells. MDA-MB-231 cells were incubated for 5 h on gelatin matrix. (A) Gelatin matrix was labeled with Alexa Fluor 568 antibody and the dark spots indicated degradation of the matrix by invadopodia (B) F-actin was targeted with phalloidin-Alexa Fluor 647, which localized to proteolytic sites on the matrix (C) In control cells the GFP was observed as a highly diffuse signal from the cell nucleus and the surrounding sytoplasm. A red arrow indicates the location of an invadopodium. Bar, 10 µm. The images were acquired with fluorescent microscopy using a 63x/1.4 N. oil immersion objective.

Similarly to control cells, F-actin was observed as bright spots in the corresponding sites of matrix degradation in MIM, ABBA and IRTKS expressing cells (Fig. 10 A and B, 11 A and B, 12 A and B). I-BAR domain proteins showed diffuse localization in most of the cells (data not shown). However, in a fraction of the cells the I-BAR domain proteins partially localized to invadopodia in the similar manner to F-actin (Fig. 10 C and D, 11 C and D and 12 C and

D). The tendency for I-BAR domain protein localization in invadopodia was seen for MIM, ABBA and IRTKS, but not in cancer cells expressing IRSp53.

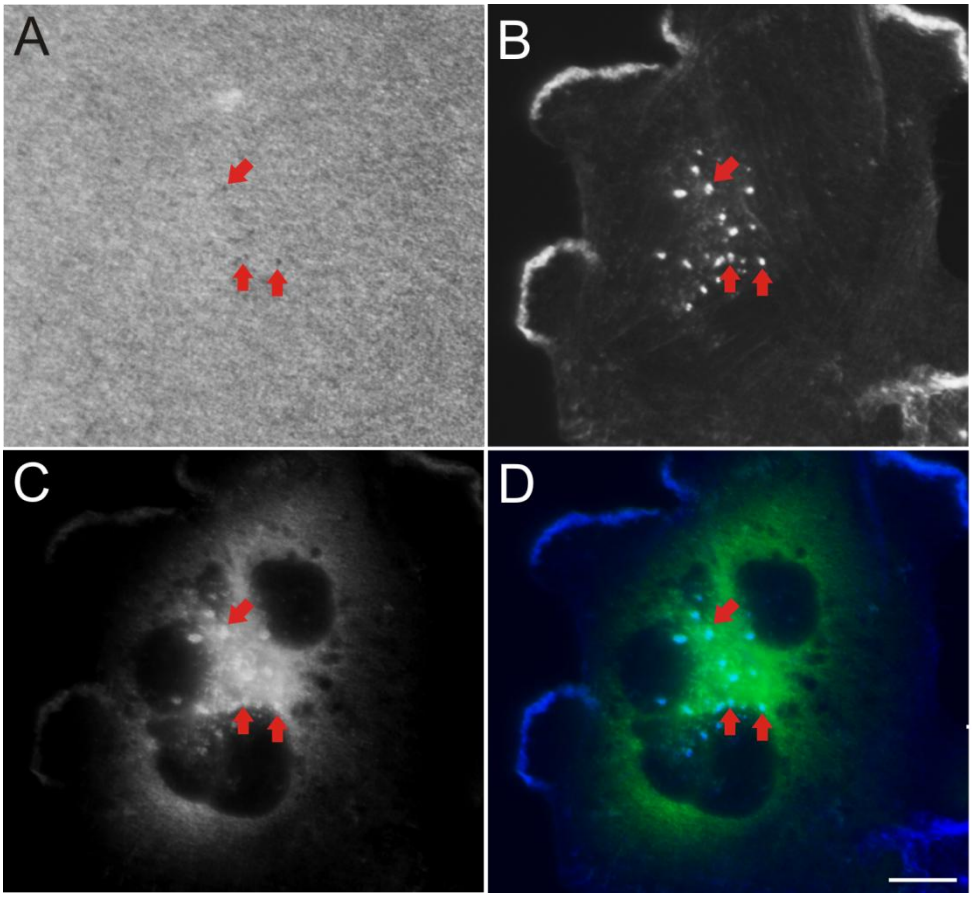

Figure 10. Fluorescent gelatin matrix degradation by invadopodia of MIM-GFP transfected MDA-MB-231 cells. Breast cancer cells were incubated for 5 h on gelatin matrix. (A) Invadopodia-mediated proteolysis of the matrix labeled with Alexa Fluor 568 antibody. (B) F-actin of invadopodia labeled with phalloidin-Alexa Fluor 647 localized to degraded sites on the matrix. (C) In this particular cell expressing MIM-GFP the fusion protein localized to invadopodia (D) A merge picture was obtained by combining channels B and C showing the accumulation of MIM-GFP and F-actin at the same sites. An invadopodium is shown by an arrow. Bar, 10 μm. The images were acquired with Zeiss fluorescent microscope using a 63x/1.4 N. oil immersion objective.

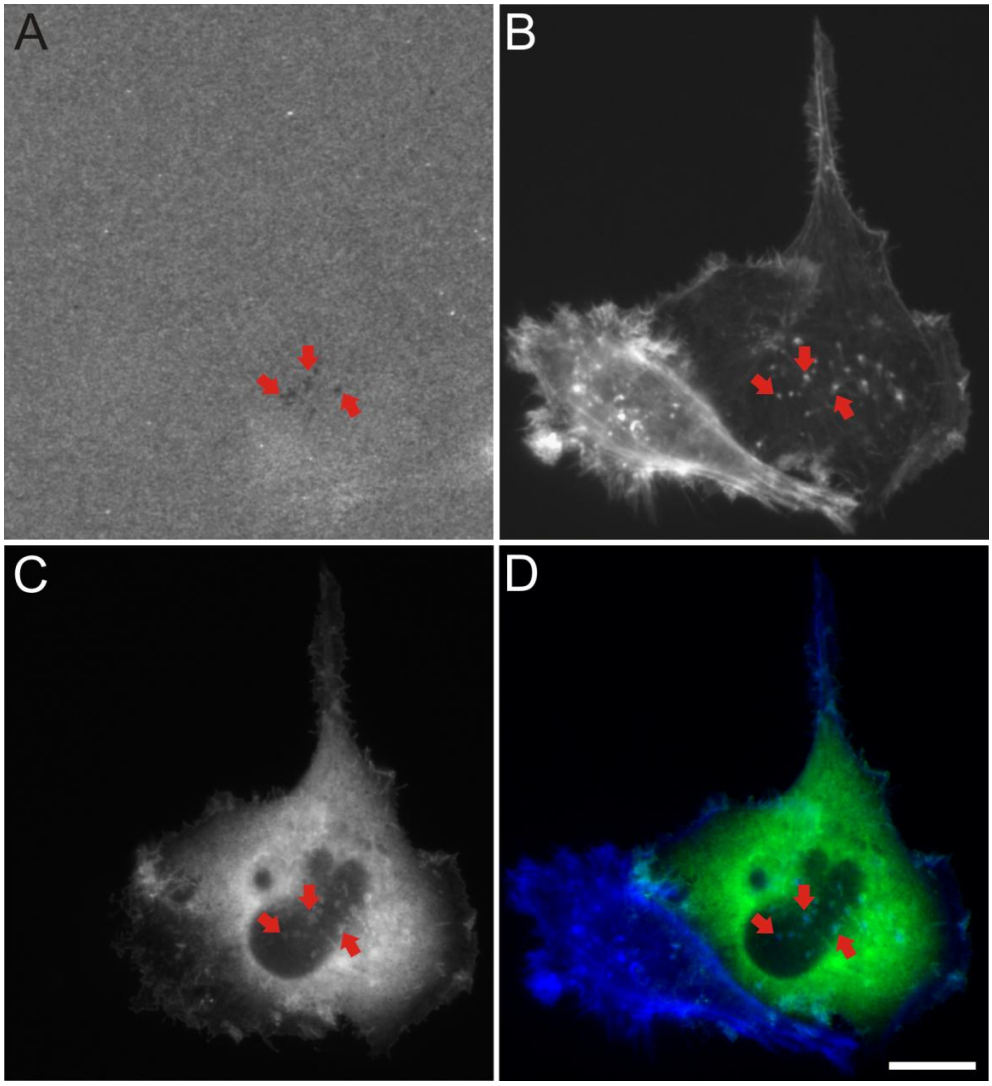

Figure 11. Gelatin matrix degradation by invadopodia of ABBA-GFP transfected MDA-MB-231 cells. The cells were incubated for 5 h on gelatin matrix. (A) Degradation of fluorescently labeled gelatin, which corresponded to the sites of F-actin labeled with phalloidin-Alexa Fluor 647 (shown in panel B). (C) The GFP signal representing ABBA localized to invadopodia. (D) Channels from figures B and C were combined and the merging shows the colocalization of ABBA and F-actin. Red arrows represent the sites of invadopodia. Bar, 10 μm. The images were acquired with Zeiss fluorescent microscope using a 63x/1.4 N. oil immersion objective.

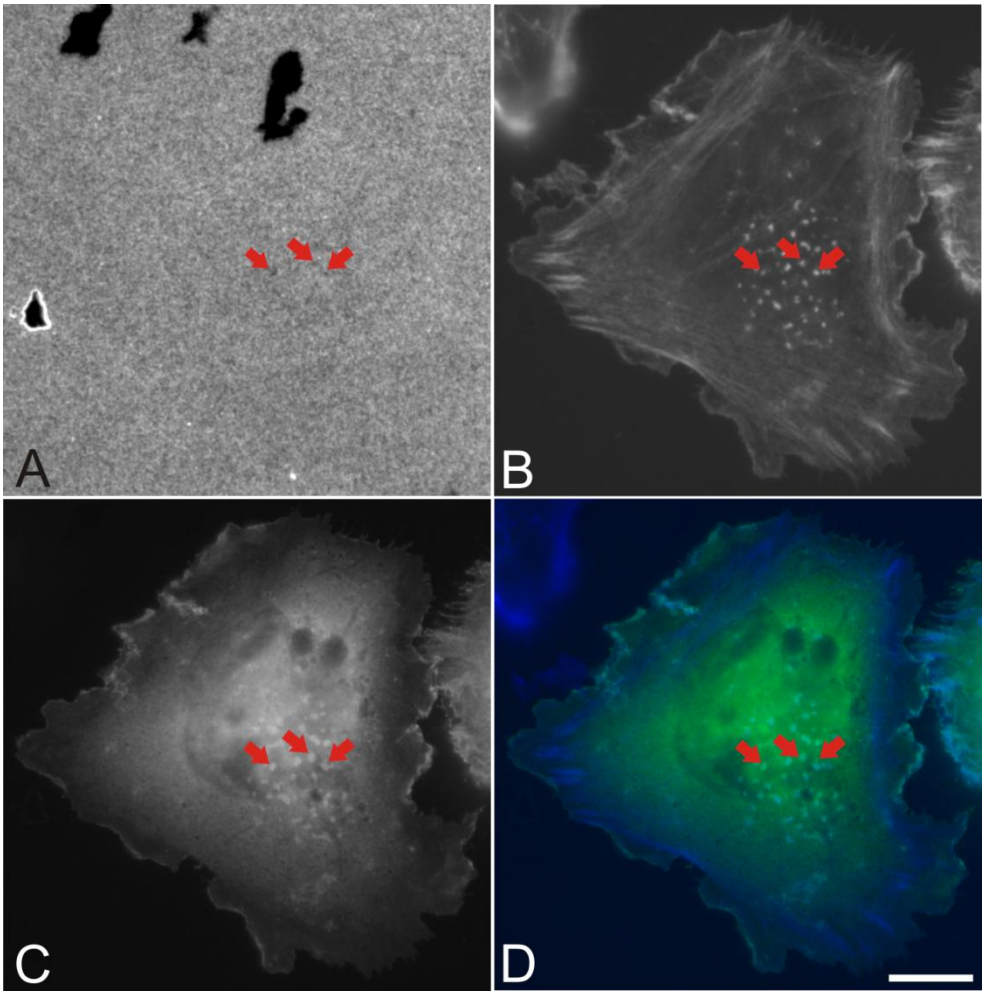

Figure 12. The proteolytic matrix degradation by invadopodia of IRTKS-GFP expressing MDA-MB231 cells. The cells were incubated for 5 h on gelatin matrix before their fixation. (A) Degradation of fluorescent matrix by invadopodia, (B) Phalloidin-Alexa Fluor 647 labeled F-actin and IRTKS localized to the sites of matrix degradation (shown in panel C). (D) A merge picture obtained by combining the channels B and C. IRTKS and F-actin colocalized at the same sites. Red arrows indicate invadopodia. Bar, 10 µm. The images were acquired with Zeiss fluorescent microscope using a 63x/1.4 N. oil immersion objective.

1.23 ECM degradation by invadopodia of glioma cells

The glioma cells were incubated for 3 hours on gelatin matrix before fixation and immunostaining with anti-ABBA-rabbit antibody. Like in breast cancer cells, the matrix degradation was observed as dark dots on the matrix underlying glioma cells and F-actin seemed to form similar kind of bright dots in the corresponding sites (Fig. 13 A and B). However, the efficiency of glioma cells to produce invadopodia per each invadopodia forming cell was ~20% lower as compared to the more invasive breast cancer cell line MDA-MB-231. Similarly to the breast cancer cells, the endogenous ABBA did not localize at sites of invadopodia in glioma cell line (Fig. 13 C).

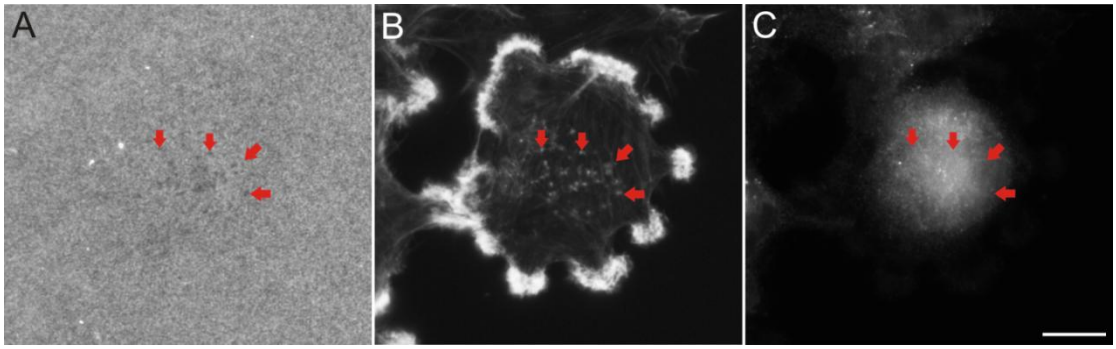

Figure 13. Degradation of Alexa 568 labeled fluorescent gelatin matrix by invadopodia of glioma SNB-19 cells. The cells were incubated on gelatin matrix for 3 hours before fixation. (A) The figure shows invadopodia-mediated gelatin matrix degradation. (B) Phalloidin-Alexa Fluor 647 labeled F-actin localized in the degradation sites. (C) Endogenous ABBA was revealed by anti-ABBA-rabbit antibody, which did not show clear accumulation at the sites of invadopodia. Red arrows indicate the sites of invadopodia. Bar, 10 µm. The images were acquired with Zeiss fluorescence microscope using a 63x/1.4 N. oil immersion objective.

1.24 Intensity profiles of invadopodia

The intensity profiles were measured for invadopodia in MDA-MB-231 cells expressing I-BAR-GFP or GFP-N1 as described in Table 1. A schematic illustration shows the distinct patterns of GFP accumulation against the signals obtained from F-actin and gelatin matrix (Table 1 A-C). The intensity profiles revealed that the fluorescent signal corresponding to the I-BAR domain protein was observed either on the invadopodia edges or at the centre of an invadopodium (Table 1 A and B). Table 1 D summarizes the results obtained from all invadopodia of I-BAR domain protein expressing cells selected for intensity profile measurements. In IRSp53 expressing cells, 2% of total invadopodia had accumulation of IRSp53 at the edges of invadopodia. In MIM-, ABBA- and IRTKS-GFP transfected cells, the corresponding percentage was higher: 6 %, 8 % and 4 %, respectively. Interestingly, only the cells expressing MIM-GFP showed GFP accumulation at the centre of an invadopodium. These invadopodia comprised of 9 % of total invadopodia in MIM-GFP expressing cells. In GFP-N1 transfected control cells, GFP accumulation in invadopodia was not detected.

By using similar intensity profile analysis, the accumulation of an antibody signal was not observed in invadopodia of MDA-MB-231 and SNB-19 cells labeled against I-BAR domain antibodies.

Table 1. Results from intensity profile measurements of distinct I-BAR domain protein constructs. Five cells per each I-BAR-GFP construct were used for determining the I-BAR domain protein accumulation in invadopodia. The distinct protein accumulation patterns obtained from the experiment are represented by a schematic illustration (A-C). F-actin is shown as a blue line, while red and green colors indicate intensity signals from the matrix and GFP, respectively. (D) The protein accumulated on the edges of an invadopodium in a fraction of cells expressing the GFP-fusion of the I-BAR domain proteins, while similar accumulation was not observed in control cells. In addition, MIM accumulation was also detected at the centre of an invadopodium.

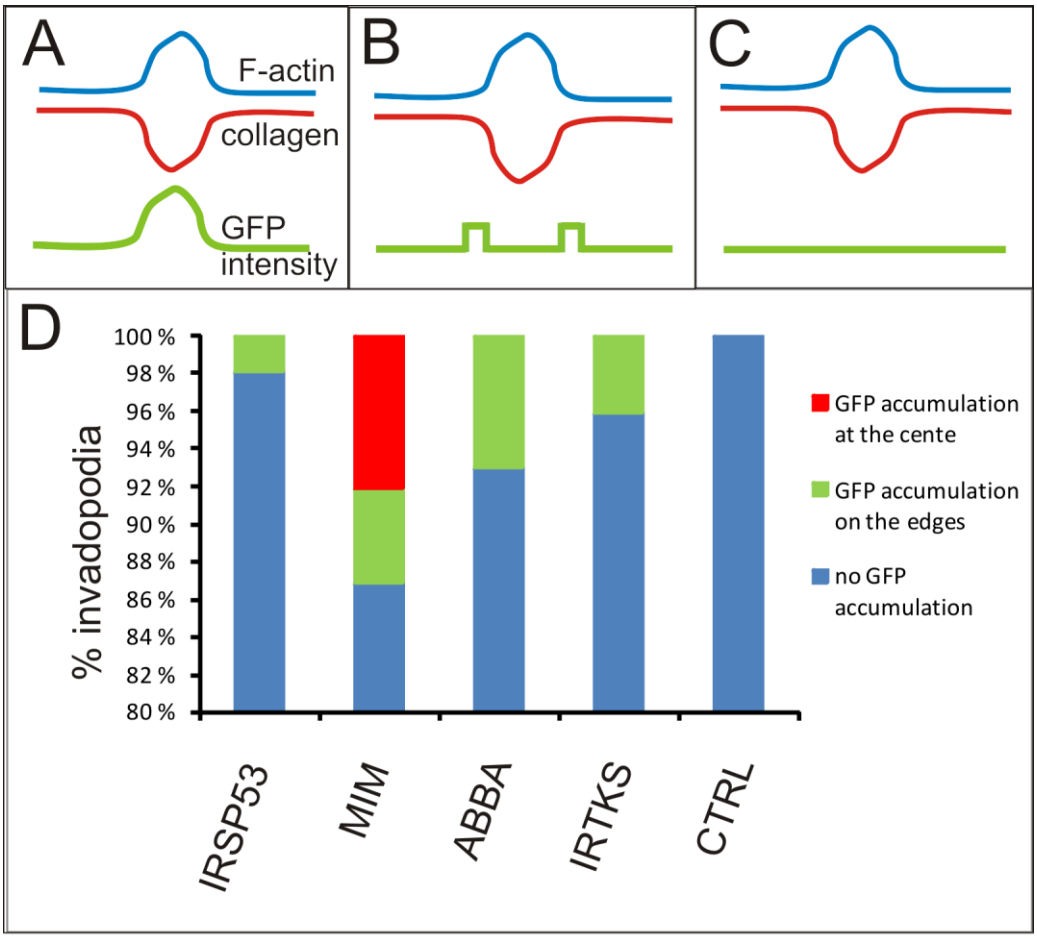

Discussion

In the present study, I have explored the localization of I-BAR domain proteins in invadopodia of invasive breast cancer and glioma cells. First, I determined the mRNA expression levels of distinct I-BAR domain proteins in MDA-MB-231 and SNB-19 cells. I found that all I-BAR domain proteins excluding FLJ22582 were expressed in both cell lines. The lack of FLJ22582 expression in these cells is in line with the recent findings from Lappalainen laboratory, demonstrating that this protein is specifically expressed in intestinal epithelial cells (Pykäläinen et al., 2011)

Next, I determined the levels of expression of ABBA, IRSp53 and IRTKS proteins in these cells by Western blotting. The results correlated with RT-PCR results and showed that all of these proteins were expressed in both cell lines. ABBA was expressed more strongly in glioma cells than in breast cancer cells both at the mRNA and protein level. The result is supported by the previous studies by Saarikangas et al. (2008), which showed that ABBA was strongly expressed in radial glial cells. Interestingly, fragments of different size corresponding to IRTKS and IRSp53 were detected both by RT-PCR and immunoblotting indicating that these two I-BAR domain proteins have different splice variants in glioma cells. Additionally, different splice variants of IRSp53 also appear to be expressed in breast cancer cells. However, IRTKS splice variants were not detected in breast cancer cells suggesting that IRTKS expression differs slightly between these two invasive cancer cell lines.

In order to study the role of these proteins in invasive motility of cancer cells, I established an ECM degradation assay, which has been previously described by Artym et al. (2009). As in the previous studies commented by Albiges-Rizo et al. (2009), invadopodia were observed as irregular dots at the centre of ventral surface of the cell, where traction forces are lower. We have confirmed here the previous observations (Chuang et al., 2004; Hashimoto et al., 2004; Artym et al., 2006) that both MDA-MB-231 and SNB-19 cell lines are able to induce invadopodia. However, invadopodia were observed more frequently in breast cancer cells than in the glioma cell line, which is consistent with the fact that gliomas lack metastatic properties.

Furthermore, glioma cells likely have other mechanisms, which drive their invasion in the central nervous system.

I also examined the localization of I-BAR domain proteins in invadopodia structures. The localization of endogenous ABBA, IRTKS and IRSp53 was explored both in 2D and 3D environment. The antibody staining was evenly distributed in all parts of the cell and hence, the localization of ABBA in those cells was impossible to determine. However in 3D cortactin and F-actin stainings were strongest at the front of the cell, which suggests that invadopodia may exist at these sites. Unfortunately, the existence of invadopodia by matrix degradation could not be confirmed with confocal microcopic methods due to strong coverslip reflection.

The strong expression of I-BAR domain proteins in brain has been previously detected (Okamura-Oho et al., 2001; Saarikangas et al., 2008) and therefore ABBA localization in glioma cells was studied. Nevertheless, similarly to breast cancer cells the antibody was evenly distributed in glioma cells indicating that the antibody recognition against endogenous ABBA was insufficient in both cell lines. Moreover, the intensity profiles analyzed for antibodies targeted against endogenous I-BAR domain proteins in breast cancer and glioma cell lines showed no accumulation of I-BAR domain protein. These studies contrasted the results obtained from the studies performed with GFP tagged I-BAR domain proteins. Overall, although the antibody recognized I-BAR domain proteins on Western blot, the immunolabeling studies suggest that the antibodies used in this study for detecting I-BAR domain proteins are not suitable for immunocytochemical applications in SNB-19 and MDA-MB-231 cells. Alternatively, because invadopodia may be very protein-dense structures, the epitopes for the membrane-associated I-BAR domains may not be accessible for the antibodies using the method applied in this study. Therefore, one possibility would be to treat the cells with denaturing chemicals that reveal the epitopes for antibody recognition.

Last, the fluorescent microscopic observations revealed that in MDA-MB-231 cells ABBA, MIM, IRTKS GFP-fusion proteins localized to invadopodia. Based on visual observations, IRSp53 did not show as clear localization to invadopodia as the other I-BAR domain proteins,

but nevertheless the intensity profile measurements revealed IRSp53 accumulation in invadopodia, yet to lesser extent. Overall, the intensity profile results revealed two kinds of I-BAR domain protein accumulation patterns in invadopodia, i.e. the I-BAR domain proteins accumulated either at the centre or at the edges of an invadopodium. The number of invadopodia showing tendency of I-BAR domain protein accumulation was low indicating that generally this is a fairly rare event. It is possible that the I-BAR domain proteins accumulate to invadopodia only during specific stages of their function/life-cycle. However, the results obtained in this study should be confirmed with immunolabeling studies as the GFP tag may disturb the natural recruitment of I-BAR domain proteins during invadopodia formation.

Vingdassalom et al. (2009) reported that IRSp53 and IRTKS contributed to pedestal formation, which is a bacterium-induced protrusive structure that shares similarities with invadopodia. My results propose that invadopodia might be formed in a similar manner in mammalian cells, where I-BAR domain proteins could serve as linkers between the actin cytoskeleton and the plasma membrane. Further, the results showing that MIM, ABBA and IRTKS localize to invadopodia, and are found more frequently from invadopodia in comparison to IRSp53, suggest that in mammalian cells they may be more essential in the formation of invadopodia than IRSp53. This proposal correlates with the results Vingdassalom et al. (2009) obtained for IRSp53 and IRTKS in bacterial pedestals.

During the initiation of membrane tubules the I-BAR domain proteins possibly form a ring-like structure on the edges of a developing invadopodium recruiting and activating N-WASP, which eventually leads to actin polymerization via Arp2/3. The observation that I-BAR domain proteins sometimes appear at the centre of an invadopodium may refer to a later stage in invadopodium formation, where the parallel actin bundles are replaced by the branched actin network. In mature invadopodia, I-BAR domain proteins might be replaced by other factors or simply dissociate from the invadopodia site. This hypothesis is supported by our studies showing that the accumulation of I-BAR domain protein is not detected in most of the invadopodia. However, more studies including live cell imaging and small interfering RNA

experiments should be conducted to reveal the actual I-BAR domain protein function and dynamics in invadopodia.

References

Alberts, B., Johnson, A., Lewis, J., Raff, M., Roberts, K., and Walter, P. (2008). Molecular Biology of the Cell, fifth edition. Garland Publishing, Inc. New York.

Albiges-Rizo, C., O. Destaing, B. Fourcade, E. Planus, and M.R. Block. 2009. Actin machinery and mechanosensitivity in invadopodia, podosomes and focal adhesions. *J.Cell.Sci.* 122:3037-3049. doi: 10.1242/jcs.052704.

Amann, K.J., and T.D. Pollard. 2001. The Arp2/3 complex nucleates actin filament branches from the sides of pre-existing filaments. *Nat.Cell Biol.* 3:306-310. doi: 10.1038/35060104.

Anand, P., A.B. Kunnumakkara, C. Sundaram, K.B. Harikumar, S.T. Tharakan, O.S. Lai, B. Sung, and B.B. Aggarwal. 2008. Cancer is a preventable disease that requires major lifestyle changes. *Pharm.Res.* 25:2097-2116. doi: 10.1007/s11095-008-9661-9.

Angers-Loustau, A., R. Hering, T.E. Werbowetski, D.R. Kaplan, and R.F. Del Maestro. 2004. SRC regulates actin dynamics and invasion of malignant glial cells in three dimensions. *Mol.Cancer.Res.* 2:595-605.

Artym, V.V., K.M. Yamada, and S.C. Mueller. 2009. ECM degradation assays for analyzing local cell invasion. *Methods Mol.Biol.* 522:211-219. doi: 10.1007/978-1-59745-413-1_15.

Artym, V.V., Y. Zhang, F. Seillier-Moiseiwitsch, K.M. Yamada, and S.C. Mueller. 2006. Dynamic interactions of cortactin and membrane type 1 matrix metalloproteinase at invadopodia: defining the stages of invadopodia formation and function. *Cancer Res.* 66:3034-3043. doi: 10.1158/0008-5472.CAN-05-2177.

Badowski, C., G. Pawlak, A. Grichine, A. Chabadel, C. Oddou, P. Jurdic, M. Pfaff, C. Albiges-Rizo, and M.R. Block. 2008. Paxillin phosphorylation controls invadopodia/podosomes spatiotemporal organization. *Mol.Biol.Cell.* 19:633-645. doi: 10.1091/mbc.E06-01-0088.

Baldassarre, M., I. Ayala, G. Beznoussenko, G. Giacchetti, L.M. Machesky, A. Luini, and R. Buccione. 2006. Actin dynamics at sites of extracellular matrix degradation. *Eur.J.Cell Biol.* 85:1217-1231. doi: 10.1016/j.ejcb.2006.08.003.

Bharti, S., H. Inoue, K. Bharti, D.S. Hirsch, Z. Nie, H.Y. Yoon, V. Artym, K.M. Yamada, S.C. Mueller, V.A. Barr, and P.A. Randazzo. 2007. Src-dependent phosphorylation of ASAP1 regulates podosomes. *Mol.Cell.Biol.* 27:8271-8283. doi: 10.1128/MCB.01781-06.

Bourguignon, L.Y., Z. Gunja-Smith, N. Iida, H.B. Zhu, L.J. Young, W.J. Muller, and R.D. Cardiff. 1998. CD44v(3,8-10) is involved in cytoskeleton-mediated tumor cell migration and matrix metalloproteinase (MMP-9) association in metastatic breast cancer cells. *J.Cell.Physiol.* 176:206-215. doi: 2-3.

Bowden, E.T., M. Barth, D. Thomas, R.I. Glazer, and S.C. Mueller. 1999. An invasion-related complex of cortactin, paxillin and PKCmu associates with invadopodia at sites of extracellular matrix degradation. *Oncogene.* 18:4440-4449. doi: 10.1038/sj.onc.1202827.

Bray, D. (2001). Cell movements: from molecules to motility. Second edition. Garland Publishing, New York.

Buccione, R., J.D. Orth, and M.A. McNiven. 2004. Foot and mouth: podosomes, invadopodia and circular dorsal ruffles. *Nat.Rev.Mol.Cell Biol.* 5:647-657. doi: 10.1038/nrm1436.

Burgstaller, G., and M. Gimona. 2005. Podosome-mediated matrix resorption and cell motility in vascular smooth muscle cells. *Am.J.Physiol.Heart Circ.Physiol.* 288:H3001-5. doi: 10.1152/ajpheart.01002.2004.

Burns, S., A.J. Thrasher, M.P. Blundell, L. Machesky, and G.E. Jones. 2001. Configuration of human dendritic cell cytoskeleton by Rho GTPases, the WAS protein, and differentiation. *Blood.* 98:1142-1149.

Campellone, K.G., D. Robbins, and J.M. Leong. 2004. EspFU is a translocated EHEC effector that interacts with Tir and N-WASP and promotes Nck-independent actin assembly. *Dev.Cell.* 7:217-228. doi: 10.1016/j.devcel.2004.07.004.

Carlson, B.R., K.E. Lloyd, A. Kruszewski, I.H. Kim, R.M. Rodriguiz, C. Heindel, M. Faytell, S.M. Dudek, W.C. Wetsel, and S.H. Soderling. 2011. WRP/srGAP3 facilitates the initiation of spine development by an inverse F-BAR domain, and its loss impairs long-term memory. *J.Neurosci.* 31:2447-2460. doi: 10.1523/JNEUROSCI.4433-10.2011.

Chen, W.T. 1996. Proteases associated with invadopodia, and their role in degradation of extracellular matrix. *Enzyme Protein.* 49:59-71.

Chen, W.T. 1989. Proteolytic activity of specialized surface protrusions formed at rosette contact sites of transformed cells. *J.Exp.Zool.* 251:167-185. doi: 10.1002/jez.1402510206.

Chen, W.T., K. Olden, B.A. Bernard, and F.F. Chu. 1984. Expression of transformation-associated protease(s) that degrade fibronectin at cell contact sites. *J.Cell Biol.* 98:1546-1555.

Choi, J., J. Ko, B. Racz, A. Burette, J.R. Lee, S. Kim, M. Na, H.W. Lee, K. Kim, R.J. Weinberg, and E. Kim. 2005. Regulation of dendritic spine morphogenesis by insulin receptor substrate 53, a downstream effector of Rac1 and Cdc42 small GTPases. *J.Neurosci.* 25:869-879. doi: 10.1523/JNEUROSCI.3212-04.2005.

Chuang, Y.Y., N.L. Tran, N. Rusk, M. Nakada, M.E. Berens, and M. Symons. 2004. Role of synaptojanin 2 in glioma cell migration and invasion. *Cancer Res.* 64:8271-8275. doi: 10.1158/0008-5472.CAN-04-2097.

Clark, E.S., A.S. Whigham, W.G. Yarbrough, and A.M. Weaver. 2007. Cortactin is an essential regulator of matrix metalloproteinase secretion and extracellular matrix degradation in invadopodia. *Cancer Res.* 67:4227-4235. doi: 10.1158/0008-5472.CAN-06-3928.

Coopman, P.J., D.M. Thomas, K.R. Gehlsen, and S.C. Mueller. 1996. Integrin alpha 3 beta 1 participates in the phagocytosis of extracellular matrix molecules by human breast cancer cells. *Mol.Biol.Cell.* 7:1789-1804.

Deryugina, E.I., B. Ratnikov, E. Monosov, T.I. Postnova, R. DiScipio, J.W. Smith, and A.Y. Strongin. 2001. MT1-MMP initiates activation of pro-MMP-2 and integrin alphavbeta3 promotes maturation of MMP-2 in breast carcinoma cells. *Exp.Cell Res.* 263:209-223. doi: 10.1006/excr.2000.5118.

Destaing, O., F. Saltel, J.C. Geminard, P. Jurdic, and F. Bard. 2003. Podosomes display actin turnover and dynamic self-organization in osteoclasts expressing actin-green fluorescent protein. *Mol.Biol.Cell.* 14:407-416. doi: 10.1091/mbc.E02-07-0389.

Evans, J.G., I. Correia, O. Krasavina, N. Watson, and P. Matsudaira. 2003. Macrophage podosomes assemble at the leading lamella by growth and fragmentation. *J.Cell Biol.* 161:697-705. doi: 10.1083/jcb.200212037.

Frost, A., V.M. Unger, and P. De Camilli. 2009. The BAR domain superfamily: membrane-molding macromolecules. *Cell.* 137:191-196. doi: 10.1016/j.cell.2009.04.010.

Gallop, J.L., C.C. Jao, H.M. Kent, P.J. Butler, P.R. Evans, R. Langen, and H.T. McMahon. 2006. Mechanism of endophilin N-BAR domain-mediated membrane curvature. *EMBO J.* 25:2898-2910. doi: 10.1038/sj.emboj.7601174.

Ghosh, M., X. Song, G. Mouneimne, M. Sidani, D.S. Lawrence, and J.S. Condeelis. 2004. Cofilin promotes actin polymerization and defines the direction of cell motility. *Science.* 304:743-746. doi: 10.1126/science.1094561.

Gonzalez-Quevedo, R., M. Shoffer, L. Horng, and A.E. Oro. 2005. Receptor tyrosine phosphatase-dependent cytoskeletal remodeling by the hedgehog-responsive gene MIM/BEG4. *J.Cell Biol.* 168:453-463. doi: 10.1083/jcb.200409078.

Govind, S., R. Kozma, C. Monfries, L. Lim, and S. Ahmed. 2001. Cdc42Hs facilitates cytoskeletal reorganization and neurite outgrowth by localizing the 58-kD insulin receptor substrate to filamentous actin. *J.Cell Biol.* 152:579-594.

Guerrier, S., J. Coutinho-Budd, T. Sassa, A. Gresset, N.V. Jordan, K. Chen, W.L. Jin, A. Frost, and F. Polleux. 2009. The F-BAR domain of srGAP2 induces membrane protrusions required for neuronal migration and morphogenesis. *Cell.* 138:990-1004. doi: 10.1016/j.cell.2009.06.047.

Gupta, G.P., and J. Massague. 2006. Cancer metastasis: building a framework. *Cell.* 127:679-695. doi: 10.1016/j.cell.2006.11.001.

Hai, C.M., P. Hahne, E.O. Harrington, and M. Gimona. 2002. Conventional protein kinase C mediates phorbol-dibutyrate-induced cytoskeletal remodeling in a7r5 smooth muscle cells. *Exp.Cell Res.* 280:64-74.

Hanahan, D., and R.A. Weinberg. 2011. Hallmarks of cancer: the next generation. *Cell.* 144:646-674. doi: 10.1016/j.cell.2011.02.013.

Hashimoto, S., Y. Onodera, A. Hashimoto, M. Tanaka, M. Hamaguchi, A. Yamada, and H. Sabe. 2004. Requirement for Arf6 in breast cancer invasive activities. *Proc.Natl.Acad.Sci.U.S.A.* 101:6647-6652. doi: 10.1073/pnas.0401753101.

Ho, H.Y., R. Rohatgi, A.M. Lebensohn, M. Le, J. Li, S.P. Gygi, and M.W. Kirschner. 2004. Toca-1 mediates Cdc42-dependent actin nucleation by activating the N-WASP-WIP complex. *Cell.* 118:203-216. doi: 10.1016/j.cell.2004.06.027.

Imai, K., E. Ohuchi, T. Aoki, H. Nomura, Y. Fujii, H. Sato, M. Seiki, and Y. Okada. 1996. Membrane-type matrix metalloproteinase 1 is a gelatinolytic enzyme and is secreted in a complex with tissue inhibitor of metalloproteinases 2. *Cancer Res.* 56:2707-2710.

Itoh, T., K.S. Erdmann, A. Roux, B. Habermann, H. Werner, and P. De Camilli. 2005. Dynamin and the actin cytoskeleton cooperatively regulate plasma membrane invagination by BAR and F-BAR proteins. *Dev.Cell.* 9:791-804. doi: 10.1016/j.devcel.2005.11.005.

Itoh, T., J. Hasegawa, K. Tsujita, Y. Kanaho, and T. Takenawa. 2009. The tyrosine kinase Fer is a downstream target of the PLD-PA pathway that regulates cell migration. *Sci.Signal.* 2:ra52. doi: 10.1126/scisignal.2000393.

Jemal, A., F. Bray, M.M. Center, J. Ferlay, E. Ward, and D. Forman. 2011. Global cancer statistics. *CA Cancer.J.Clin.* doi: 10.3322/caac.20107.

Kelly, T., S.C. Mueller, Y. Yeh, and W.T. Chen. 1994. Invadopodia promote proteolysis of a wide variety of extracellular matrix proteins. *J.Cell.Physiol.* 158:299-308. doi: 10.1002/jcp.1041580212.

Kelly, T., Y. Yan, R.L. Osborne, A.B. Athota, T.L. Rozypal, J.C. Colclasure, and W.S. Chu. 1998. Proteolysis of extracellular matrix by invadopodia facilitates human breast cancer cell invasion and is mediated by matrix metalloproteinases. *Clin.Exp.Metastasis.* 16:501-512.

Kikuchi, K., and K. Takahashi. 2008. WAVE2- and microtubule-dependent formation of long protrusions and invasion of cancer cells cultured on three-dimensional extracellular matrices. *Cancer.Sci.* 99:2252-2259. doi: 10.1111/j.1349-7006.2008.00927.x.

Kiuchi, T., K. Ohashi, S. Kurita, and K. Mizuno. 2007. Cofilin promotes stimulus-induced lamellipodium formation by generating an abundant supply of actin monomers. *J.Cell Biol.* 177:465-476. doi: 10.1083/jcb.200610005.

Krugmann, S., I. Jordens, K. Gevaert, M. Driessens, J. Vandekerckhove, and A. Hall. 2001. Cdc42 induces filopodia by promoting the formation of an IRSp53:Mena complex. *Curr.Biol.* 11:1645-1655.

Lappalainen, P., and D.G. Drubin. 1997. Cofilin promotes rapid actin filament turnover in vivo. *Nature.* 388:78-82. doi: 10.1038/40418.

Lee, S.H., F. Kerff, D. Chereau, F. Ferron, A. Klug, and R. Dominguez. 2007. Structural basis for the actin-binding function of missing-in-metastasis. *Structure.* 15:145-155. doi: 10.1016/j.str.2006.12.005.

Lee, Y.G., J.A. Macoska, S. Korenchuk, and K.J. Pienta. 2002. MIM, a potential metastasis suppressor gene in bladder cancer. *Neoplasia.* 4:291-294. doi: 10.1038/sj.neo.7900231.

Lengauer, C., K.W. Kinzler, and B. Vogelstein. 1998. Genetic instabilities in human cancers. *Nature.* 396:643-649. doi: 10.1038/25292.

Lewis, A.K., and P.C. Bridgman. 1992. Nerve growth cone lamellipodia contain two populations of actin filaments that differ in organization and polarity. *J.Cell Biol.* 119:1219-1243.

Lin, J., J. Liu, Y. Wang, J. Zhu, K. Zhou, N. Smith, and X. Zhan. 2005. Differential regulation of cortactin and N-WASP-mediated actin polymerization by missing in metastasis (MIM) protein. *Oncogene.* 24:2059-2066. doi: 10.1038/sj.onc.1208412.

Linder, S. 2007. The matrix corroded: podosomes and invadopodia in extracellular matrix degradation. *Trends Cell Biol.* 17:107-117. doi: 10.1016/j.tcb.2007.01.002.

Linder, S., D. Nelson, M. Weiss, and M. Aepfelbacher. 1999. Wiskott-Aldrich syndrome protein regulates podosomes in primary human macrophages. *Proc.Natl.Acad.Sci.U.S.A.* 96:9648-9653.

Liu, H., P. Radhakrishnan, L. Magoun, M. Prabu, K.G. Campellone, P. Savage, F. He, C.A. Schiffer, and J.M. Leong. 2002. Point mutants of EHEC intimin that diminish Tir recognition and actin pedestal formation highlight a putative Tir binding pocket. *Mol.Microbiol.* 45:1557-1573.

Loeb, K.R., and L.A. Loeb. 2000. Significance of multiple mutations in cancer. *Carcinogenesis.* 21:379-385.

Lorenz, M., H. Yamaguchi, Y. Wang, R.H. Singer, and J. Condeelis. 2004. Imaging sites of N-wasp activity in lamellipodia and invadopodia of carcinoma cells. *Curr.Biol.* 14:697-703. doi: 10.1016/j.cub.2004.04.008.

Machesky, L.M., and S.A. Johnston. 2007. MIM: a multifunctional scaffold protein. *J.Mol.Med.* 85:569-576. doi: 10.1007/s00109-007-0207-0.

Macias, M.J., S. Wiesner, and M. Sudol. 2002. WW and SH3 domains, two different scaffolds to recognize proline-rich ligands. *FEBS Lett.* 513:30-37.

Masuda, M., S. Takeda, M. Sone, T. Ohki, H. Mori, Y. Kamioka, and N. Mochizuki. 2006. Endophilin BAR domain drives membrane curvature by two newly identified structure-based mechanisms. *EMBO J.* 25:2889-2897. doi: 10.1038/sj.emboj.7601176.

Mattila, P.K., A. Pykalainen, J. Saarikangas, V.O. Paavilainen, H. Vihinen, E. Jokitalo, and P. Lappalainen. 2007. Missing-in-metastasis and IRSp53 deform PI(4,5)P2-rich membranes by an inverse BAR domain-like mechanism. *J.Cell Biol.* 176:953-964. doi: 10.1083/jcb.200609176.

Mattila, P.K., M. Salminen, T. Yamashiro, and P. Lappalainen. 2003. Mouse MIM, a tissue-specific regulator of cytoskeletal dynamics, interacts with ATP-actin monomers through its C-terminal WH2 domain. *J.Biol.Chem.* 278:8452-8459. doi: 10.1074/jbc.M212113200.

Mendez, M.G., S. Kojima, and R.D. Goldman. 2010. Vimentin induces changes in cell shape, motility, and adhesion during the epithelial to mesenchymal transition. *FASEB J.* 24:1838-1851. doi: 10.1096/fj.09-151639.

Miki, H., H. Yamaguchi, S. Suetsugu, and T. Takenawa. 2000. IRSp53 is an essential intermediate between Rac and WAVE in the regulation of membrane ruffling. *Nature.* 408:732-735. doi: 10.1038/35047107.

Millard, T.H., G. Bompard, M.Y. Heung, T.R. Dafforn, D.J. Scott, L.M. Machesky, and K. Futterer. 2005. Structural basis of filopodia formation induced by the IRSp53/MIM homology domain of human IRSp53. *EMBO J.* 24:240-250. doi: 10.1038/sj.emboj.7600535.

Millard, T.H., J. Dawson, and L.M. Machesky. 2007. Characterisation of IRTKS, a novel IRSp53/MIM family actin regulator with distinct filament bundling properties. *J.Cell.Sci.* 120:1663-1672. doi: 10.1242/jcs.001776.

Mizutani, K., H. Miki, H. He, H. Maruta, and T. Takenawa. 2002. Essential role of neural Wiskott-Aldrich syndrome protein in podosome formation and degradation of extracellular matrix in src-transformed fibroblasts. *Cancer Res.* 62:669-674.

Mueller, S.C., and W.T. Chen. 1991. Cellular invasion into matrix beads: localization of beta 1 integrins and fibronectin to the invadopodia. *J.Cell.Sci.* 99 (Pt 2):213-225.

Mueller, S.C., G. Ghersi, S.K. Akiyama, Q.X. Sang, L. Howard, M. Pineiro-Sanchez, H. Nakahara, Y. Yeh, and W.T. Chen. 1999. A novel protease-docking function of integrin at invadopodia. *J.Biol.Chem.* 274:24947-24952.

Mueller, S.C., Y. Yeh, and W.T. Chen. 1992. Tyrosine phosphorylation of membrane proteins mediates cellular invasion by transformed cells. *J.Cell Biol.* 119:1309-1325.

Mullins, R.D., J.A. Heuser, and T.D. Pollard. 1998. The interaction of Arp2/3 complex with actin: nucleation, high affinity pointed end capping, and formation of branching networks of filaments. *Proc.Natl.Acad.Sci.U.S.A.* 95:6181-6186.

Nakagawa, H., H. Miki, M. Nozumi, T. Takenawa, S. Miyamoto, J. Wehland, and J.V. Small. 2003. IRSp53 is colocalised with WAVE2 at the tips of protruding lamellipodia and filopodia independently of Mena. *J.Cell.Sci.* 116:2577-2583. doi: 10.1242/jcs.00462.

Nakagawa, S., and M. Takeichi. 1995. Neural crest cell-cell adhesion controlled by sequential and subpopulation-specific expression of novel cadherins. *Development.* 121:1321-1332.

Nakahara, H., L. Howard, E.W. Thompson, H. Sato, M. Seiki, Y. Yeh, and W.T. Chen. 1997. Transmembrane/cytoplasmic domain-mediated membrane type 1-matrix metalloprotease docking to invadopodia is required for cell invasion. *Proc.Natl.Acad.Sci.U.S.A.* 94:7959-7964.

Nakahara, H., M. Nomizu, S.K. Akiyama, Y. Yamada, Y. Yeh, and W.T. Chen. 1996. A mechanism for regulation of melanoma invasion. Ligation of alpha6beta1 integrin by laminin G peptides. *J.Biol.Chem.* 271:27221-27224.

Nakahara, H., T. Otani, T. Sasaki, Y. Miura, Y. Takai, and M. Kogo. 2003. Involvement of Cdc42 and Rac small G proteins in invadopodia formation of RPMI7951 cells. *Genes Cells.* 8:1019-1027.

Ochoa, G.C., V.I. Slepnev, L. Neff, N. Ringstad, K. Takei, L. Daniell, W. Kim, H. Cao, M. McNiven, R. Baron, and P. De Camilli. 2000. A functional link between dynamin and the actin cytoskeleton at podosomes. *J.Cell Biol.* 150:377-389.

Okamura-Oho, Y., T. Miyashita, and M. Yamada. 2001. Distinctive tissue distribution and phosphorylation of IRSp53 isoforms. *Biochem.Biophys.Res.Commun.* 289:957-960. doi: 10.1006/bbrc.2001.6102.

Osiak, A.E., G. Zenner, and S. Linder. 2005. Subconfluent endothelial cells form podosomes downstream of cytokine and RhoGTPase signaling. *Exp.Cell Res.* 307:342-353. doi: 10.1016/j.yexcr.2005.03.035.

Paavilainen, V.O., E. Bertling, S. Falck, and P. Lappalainen. 2004. Regulation of cytoskeletal dynamics by actin-monomer-binding proteins. *Trends Cell Biol.* 14:386-394. doi: 10.1016/j.tcb.2004.05.002.

Pavlov, D., A. Muhlrad, J. Cooper, M. Wear, and E. Reisler. 2007. Actin filament severing by cofilin. *J.Mol.Biol.* 365:1350-1358. doi: 10.1016/j.jmb.2006.10.102.

Pei, D., and S.J. Weiss. 1996. Transmembrane-deletion mutants of the membrane-type matrix metalloproteinase-1 process progelatinase A and express intrinsic matrix-degrading activity. *J.Biol.Chem.* 271:9135-9140.

Peter, B.J., H.M. Kent, I.G. Mills, Y. Vallis, P.J. Butler, P.R. Evans, and H.T. McMahon. 2004. BAR domains as sensors of membrane curvature: the amphiphysin BAR structure. *Science.* 303:495-499. doi: 10.1126/science.1092586.

Pollard, T.D., and J.A. Cooper. 2009. Actin, a central player in cell shape and movement. *Science.* 326:1208-1212. doi: 10.1126/science.1175862.

Pykäläinen A, Boczkowska M, Zhao H, Saarikangas J, Rebowski G, Jansen M, Hakanen J, Koskela E V, Peränen J, Vihinen H, Jokitalo E, Salminen M, Ikonen E, Dominguez R, Lappalainen P. Pinkbar is an epithelial-specific BAR domain protein that generates planar membrane structures. Nat Struct Mol Biol. 2011. In press.

Qualmann, B., and M.M. Kessels. 2009. New players in actin polymerization--WH2-domain-containing actin nucleators. *Trends Cell Biol.* 19:276-285. doi: 10.1016/j.tcb.2009.03.004.

Rohatgi, R., L. Ma, H. Miki, M. Lopez, T. Kirchhausen, T. Takenawa, and M.W. Kirschner. 1999. The interaction between N-WASP and the Arp2/3 complex links Cdc42-dependent signals to actin assembly. *Cell.* 97:221-231.

Saarikangas, J., J. Hakanen, P.K. Mattila, M. Grumet, M. Salminen, and P. Lappalainen. 2008. ABBA regulates plasma-membrane and actin dynamics to promote radial glia extension. *J.Cell.Sci.* 121:1444-1454. doi: 10.1242/jcs.027466.

Saarikangas, J., P.K. Mattila, M. Varjosalo, M. Bovellan, J. Hakanen, J. Calzada-Wack, M. Tost, L. Jennen, B. Rathkolb, W. Hans, M. Horsch, M.E. Hyvonen, N. Perala, H. Fuchs, V. Gailus-Durner, I. Esposito, E. Wolf, M.H. de Angelis, M.J. Frilander, H. Savilahti, H. Sariola, K. Sainio, S. Lehtonen, J. Taipale, M. Salminen, and P. Lappalainen. 2011. Missing-in-metastasis MIM/MTSS1 promotes actin assembly at intercellular junctions and is required for integrity of kidney epithelia. *J.Cell.Sci.* 124:1245-1255. doi: 10.1242/jcs.082610.

Saarikangas, J., H. Zhao, and P. Lappalainen. 2010. Regulation of the actin cytoskeleton-plasma membrane interplay by phosphoinositides. *Physiol.Rev.* 90:259-289. doi: 10.1152/physrev.00036.2009.

Saarikangas, J., H. Zhao, A. Pykalainen, P. Laurinmaki, P.K. Mattila, P.K. Kinnunen, S.J. Butcher, and P. Lappalainen. 2009. Molecular mechanisms of membrane deformation by I-BAR domain proteins. *Curr.Biol.* 19:95-107. doi: 10.1016/j.cub.2008.12.029.

Schoumacher, M., R.D. Goldman, D. Louvard, and D.M. Vignjevic. 2010. Actin, microtubules, and vimentin intermediate filaments cooperate for elongation of invadopodia. *J.Cell Biol.* 189:541-556. doi: 10.1083/jcb.200909113.

Scita, G., S. Confalonieri, P. Lappalainen, and S. Suetsugu. 2008. IRSp53: crossing the road of membrane and actin dynamics in the formation of membrane protrusions. *Trends Cell Biol.* 18:52-60. doi: 10.1016/j.tcb.2007.12.002.

Shimada, A., H. Niwa, K. Tsujita, S. Suetsugu, K. Nitta, K. Hanawa-Suetsugu, R. Akasaka, Y. Nishino, M. Toyama, L. Chen, Z.J. Liu, B.C. Wang, M. Yamamoto, T. Terada, A. Miyazawa, A. Tanaka, S. Sugano, M. Shirouzu, K. Nagayama, T. Takenawa, and S. Yokoyama. 2007. Curved EFC/F-BAR-domain dimers are joined end to end into a filament for membrane invagination in endocytosis. *Cell.* 129:761-772. doi: 10.1016/j.cell.2007.03.040.

Soltau, M., K. Berhorster, S. Kindler, F. Buck, D. Richter, and H.J. Kreienkamp. 2004. Insulin receptor substrate of 53 kDa links postsynaptic shank to PSD-95. *J.Neurochem.* 90:659-665. doi: 10.1111/j.1471-4159.2004.02523.x.

Suetsugu, S., K. Murayama, A. Sakamoto, K. Hanawa-Suetsugu, A. Seto, T. Oikawa, C. Mishima, M. Shirouzu, T. Takenawa, and S. Yokoyama. 2006. The RAC binding domain/IRSp53-MIM homology domain of IRSp53 induces RAC-dependent membrane deformation. *J.Biol.Chem.* 281:35347-35358. doi: 10.1074/jbc.M606814200.

Suetsugu, S., K. Toyooka, and Y. Senju. 2010. Subcellular membrane curvature mediated by the BAR domain superfamily proteins. *Semin.Cell Dev.Biol.* 21:340-349. doi: 10.1016/j.semcdb.2009.12.002.

Svitkina, T.M., and G.G. Borisy. 1999. Arp2/3 complex and actin depolymerizing factor/cofilin in dendritic organization and treadmilling of actin filament array in lamellipodia. *J.Cell Biol.* 145:1009-1026.

Tague, S.E., V. Muralidharan, and C. D'Souza-Schorey. 2004. ADP-ribosylation factor 6 regulates tumor cell invasion through the activation of the MEK/ERK signaling pathway. *Proc.Natl.Acad.Sci.U.S.A.* 101:9671-9676. doi: 10.1073/pnas.0403531101.

Tarricone, C., B. Xiao, N. Justin, P.A. Walker, K. Rittinger, S.J. Gamblin, and S.J. Smerdon. 2001. The structural basis of Arfaptin-mediated cross-talk between Rac and Arf signalling pathways. *Nature.* 411:215-219. doi: 10.1038/35075620.

Tatin, F., C. Varon, E. Genot, and V. Moreau. 2006. A signalling cascade involving PKC, Src and Cdc42 regulates podosome assembly in cultured endothelial cells in response to phorbol ester. *J.Cell.Sci.* 119:769-781. doi: 10.1242/jcs.02787.

Tsujita, K., S. Suetsugu, N. Sasaki, M. Furutani, T. Oikawa, and T. Takenawa. 2006. Coordination between the actin cytoskeleton and membrane deformation by a novel membrane tubulation domain of PCH proteins is involved in endocytosis. *J.Cell Biol.* 172:269-279. doi: 10.1083/jcb.200508091.

van Hinsbergh, V.W., M.A. Engelse, and P.H. Quax. 2006. Pericellular proteases in angiogenesis and vasculogenesis. *Arterioscler.Thromb.Vasc.Biol.* 26:716-728. doi: 10.1161/01.ATV.0000209518.58252.17.

Vingadassalom, D., A. Kazlauskas, B. Skehan, H.C. Cheng, L. Magoun, D. Robbins, M.K. Rosen, K. Saksela, and J.M. Leong. 2009. Insulin receptor tyrosine kinase substrate links the E. coli O157:H7 actin assembly effectors Tir and EspF(U) during pedestal formation. *Proc.Natl.Acad.Sci.U.S.A.* 106:6754-6759. doi: 10.1073/pnas.0809131106.

Weiss, S.M., M. Ladwein, D. Schmidt, J. Ehinger, S. Lommel, K. Stading, U. Beutling, A. Disanza, R. Frank, L. Jansch, G. Scita, F. Gunzer, K. Rottner, and T.E. Stradal. 2009. IRSp53 links the enterohemorrhagic E. coli effectors Tir and EspFU for actin pedestal formation. *Cell.Host Microbe.* 5:244-258. doi: 10.1016/j.chom.2009.02.003.

Yamagishi, A., M. Masuda, T. Ohki, H. Onishi, and N. Mochizuki. 2004. A novel actin bundling/filopodium-forming domain conserved in insulin receptor tyrosine kinase substrate p53 and missing in metastasis protein. *J.Biol.Chem.* 279:14929-14936. doi: 10.1074/jbc.M309408200.

Yamaguchi, H., M. Lorenz, S. Kempiak, C. Sarmiento, S. Coniglio, M. Symons, J. Segall, R. Eddy, H. Miki, T. Takenawa, and J. Condeelis. 2005. Molecular mechanisms of invadopodium formation: the role of the N-WASP-Arp2/3 complex pathway and cofilin. *J.Cell Biol.* 168:441-452. doi: 10.1083/jcb.200407076.

Yeh, T.C., W. Ogawa, A.G. Danielsen, and R.A. Roth. 1996. Characterization and cloning of a 58/53-kDa substrate of the insulin receptor tyrosine kinase. *J.Biol.Chem.* 271:2921-2928.

Yilmaz, M., and G. Christofori. 2009. EMT, the cytoskeleton, and cancer cell invasion. *Cancer Metastasis Rev.* 28:15-33. doi: 10.1007/s10555-008-9169-0.

Zhao, H., A. Pykalainen, and P. Lappalainen. 2011. I-BAR domain proteins: linking actin and plasma membrane dynamics. *Curr.Opin.Cell Biol.* 23:14-21. doi: 10.1016/j.ceb.2010.10.005.

Zhao, Y., Q. Yan, X. Long, X. Chen, and Y. Wang. 2008. Vimentin affects the mobility and invasiveness of prostate cancer cells. *Cell Biochem.Funct.* 26:571-577. doi: 10.1002/cbf.1478.

Zheng, D., S. Niu, D. Yu, X.H. Zhan, X. Zeng, B. Cui, Y. Chen, J. Yoon, S.S. Martin, X. Lu, and X. Zhan. 2010. Abba promotes PDGF-mediated membrane ruffling through activation of the small GTPase Rac1. *Biochem.Biophys.Res.Commun.* 401:527-532. doi: 10.1016/j.bbrc.2010.09.087.

NCBI databank. http://www.ncbi.nlm.nih.gov/protein/NP_079321.3